

THE FLORIDA STATE UNIVERSITY  
COLLEGE OF ARTS AND SCIENCES

THE SEASONAL CIRCULATION  
OF THE UPPER OCEAN  
IN THE BAY OF BENGAL

By

JAMES T. POTE MRA

A Thesis Submitted to the  
Department of Oceanography in partial  
fulfillment of the requirements for  
the degree of Master of Science

Degree Awarded:

Fall Semester, 1990

Fall Semester, 1990

The members of the Committee approve the thesis of James T. Potemra, defended on August 31, 1990.



James J. O'Brien  
Professor Directing Thesis

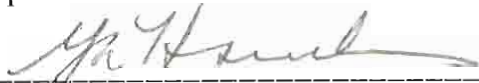


Nancy Marcus  
Committee Member



William K. Dewar  
Committee Member

Approved:



Ya Hsueh, Chair, Department of Oceanography



Ya Hsueh, Chair, Department of Oceanography

## Acknowledgements

I would like to express my sincere gratitude to the members of the Mesoscale Air-Sea Interaction Group for all their insights and helpful discussions concerning this effort. The work of Alan Davis and Dr. Mark Luther was particularly essential to the successful completion of this endeavor.

In addition, I greatly appreciate the members of my committee, Dr. William Dewar and Dr. Nancy Marcus for their help not only with this work but also for their contribution to my overall education.

Finally, and most importantly, I wish to thank my advisor, Dr. O'Brien, who was instrumental in all aspects of my graduate career at Florida State. I was only through his help and guidance that this work was possible.

## Table of Contents

	Page
Acknowledgements.....	iii
List of Figures.....	v
Abstract.....	vii
1. INTRODUCTION.....	1
2. MODEL.....	7
3. WINDS.....	16
4. REGIONAL CIRCULATION.....	26
4.1 Bay of Bengal.....	37
4.2 Andaman Sea.....	45
4.3 Equatorial Currents.....	47
5. TEMPORAL VARIATIONS.....	59
6. CONCLUSIONS.....	71
References.....	74
Biographical Sketch.....	80

## List of Figures

	Page
Figure 1. Large scale circulation as observed during (a) the winter (northeast) monsoon, and (b) the summer (southwest) monsoon.....	4
Figure 2. Model domain.....	14
Figure 3. Schematic representation of monsoon system.....	17
Figure 4a. Monthly mean wind field for January.....	20
Figure 4b. Monthly mean wind field for July.....	21
Figure 4c. Monthly mean wind field for April.....	22
Figure 4d. Monthly mean wind field for October.....	23
Figure 5. Model results for the surface layer.(a) February. (b) March. (c) May. (d) June. (e) August. (f) November.....	29
(b) March. (c) May. (d) June. (e) August. (f) November.....	29

Figure 6.	Model results for the second layer. (a) February (b) March. (c) May. (d) June. (e) August. (f) November.....	33
Figure 7.	Transect locations.....	38
Figure 8.	Mass transport in the Bay of Bengal.....	42
Figure 9.	Mass transport in the Andaman Sea.....	48
Figure 10.	Mass transport in the equatorial region.....	53
Figure 11a.	Zonal velocity in the upper layer at 18° N.....	62
Figure 11b.	Upper layer thickness at 18° N.....	63
Figure 12.	Meridional velocity in the lower layer at 13° N....	65
Figure 13.	Antisymmetric component of the height field at 3° N.....	68
Figure 14.	Meridional velocity at the equator for (a) model upper layer, and (b) model lower layer.....	69

## Abstract

Analysis of the results of a multi-layer, adiabatic, numerical model of the upper Indian Ocean, driven by climatological monthly mean winds, shows that the simulated currents in the northeastern Indian Ocean are in general agreement with available observations and interpretations. The main features of the ocean currents include large anticyclonic flow in the Bay of Bengal surface waters during the northern hemisphere winter. This gyre decays into eddies in spring and then transitions into a weaker, cyclonic gyre by late summer. The western recirculation region of this flow is an intensified western boundary current which changes direction twice during the year. In the Andaman Sea, west of the Bay of Bengal, the oceanic flow is circular. It changes direction twice during the year; it is cyclonic during the spring and early summer and anticyclonic the rest of the year. Flow in the equatorial region shows the North Equatorial Current (NEC) flowing west during winter. Further south is the eastward flowing Equatorial Counter Current (ECC) and the westward flowing South Equatorial Current (SEC). In summer, the NEC switches direction, joins the ECC, and forms the Indian Monsoon Current (IMC). Investigation of the second layer of the model (the upper 450 m of the ocean) shows that flow during much of the year is baroclinic (strong vertical

shear). Model layer thickness reveals coastal Kelvin waves propagating along the coast, traveling the entire perimeter of the Andaman Sea and the Bay of Bengal. This wave excites westward propagating Rossby waves into the interior of the bay. Time series analysis of transport calculations yield significant peaks in the 20 to 30 day range and 50 to 60 day range which are not likely directly forced by the applied wind stress (since it is monthly mean).



## 1. INTRODUCTION

The Indian Ocean circulation is a particularly interesting, dynamically rich area due to the changing wind patterns associated with the Indian Monsoon. In spite of this, it is a relatively poorly studied area. In addition, data coverage for the area is sparse. While some data sets do exist, they are predominantly on large space and time scales. Recent efforts, such as the monsoon experiment (MONEX) of the Global Atmospheric Research Program (GARP), the First GARP Global Experiment (FGGE) and the Indian Ocean Experiment (INDEX), have substantially improved the availability of measured data in this region.

Individual studies have also contributed in recent years to the understanding of the dynamics in the Indian Ocean. An early effort by *Wyrtki* [1961] is a synthesis of available data sets (at the time) of the properties of the Southeast Asian waters. More recently, *Legeckis* [1987] demonstrates the appearance of a western boundary current in the Bay of Bengal using sea surface temperature data obtained from the advanced very high resolution radiometer (AVHRR) carried on-board the NOAA-9 satellite. Data coverage from this satellite encompasses the entire Indian Ocean [*McClain et al.*, 1985]. *Rao et al.* [1989] have generated mean monthly mixed layer depth, sea surface temperature, and surface [*McClain et al.*, 1985]. *Rao et al.* [1989] have generated mean monthly mixed layer depth, sea surface temperature, and surface

current climatologies for the tropical Indian Ocean. *Molinari et al.* [1990] analyzed data sets from three different satellite-tracked, drifting buoys and compiled a monthly climatology of surface currents in the tropical Indian Ocean.

Finally, oceanic data for the Indian Ocean is compiled in a few excellent atlases [see *Düing*, 1970; *Cutler and Swallow*, 1984; *Hastenrath and Lamb*, 1979; and *Wyrcki*, 1971]. Although these sources contribute significantly to the understanding of dynamics in the tropical Indian Ocean, data on smaller scales, particularly in the Bay of Bengal, are somewhat limited.

The focus of this study, therefore, is to use a realistic, wind-driven model to simulate ocean currents in the region of the Bay of Bengal, from 75° E to 111° E and from 7° S to 23° N. Similar studies have been done for other areas of the Indian Ocean [*Jensen*, 1990] and using different models [*Woodberry et al.*, 1989]. A review of modeling efforts in the Indian Ocean can be found in *Luther* [1987]. The results of the model are compared to measured data in an attempt to understand the dynamics of the area. The model used for this study, developed at the Florida State University [*Jensen*, 1990], is a reduced gravity, three and one half layer model.

Since the model has multiple layers, the subsurface currents can be studied as well as the surface. The lowest layer is at rest, can be studied as well as the surface. The lowest layer is at rest,

however, and only the results from the first (surface) and second (subsurface) layers will be examined here.

Figure 1 shows the typical large scale circulation pattern associated with the winter and summer monsoons as compiled by *Düing* [1970]. The general surface circulation of the region, because of the seasonal wind reversal, shows a north-south symmetry at the equator only during the northern winter season (January, February, and March). During this time the monsoon winds are predominantly from the northeast (northeasterly or, equivalently, southwestward), similar to the Trade Winds in the Northern Hemisphere. In the northern summer (June, July, and August) the monsoon winds reverse their direction. The northern surface water, consequently, is entrained toward the east. Conversely, the southern waters remain in large anticyclonic flow. The result is that the three elements of the equatorial currents of the Indian Ocean are only seen during the winter monsoon [*Piccard and Emery*, 1982].

At this time, a drift current, the North Equatorial Current (NEC), is established. This current flows from east to west between  $10^{\circ}$  N and  $3^{\circ}$  S. When this current reaches Somalia on the western side of the ocean basin, it turns southward to the doldrums ( $5^{\circ}$  S). In this region, from  $3^{\circ}$  S to  $10^{\circ}$  S, the flow returns to the east as the Equatorial Counter Current (ECC). Beyond  $90^{\circ}$  E, as this current begins to weaken, it branches into two separate currents. One the Equatorial Counter Current (ECC). Beyond  $90^{\circ}$  E, as this current begins to weaken, it branches into two separate currents. One

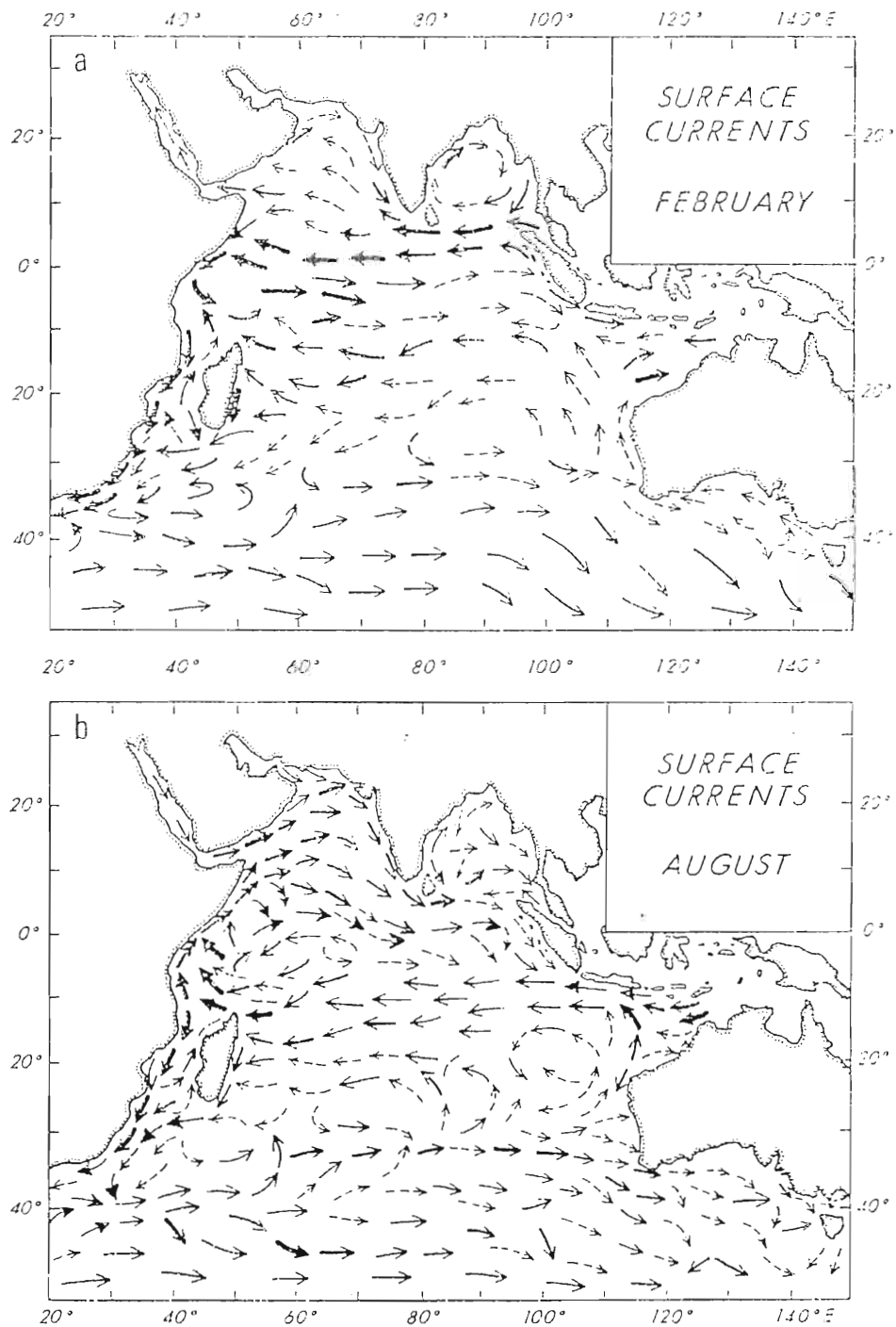


Figure 1. Large scale circulation as observed during (a) the winter (northeast) monsoon, and (b) the summer (southwest) monsoon. (courtesy of W. Düing)

Figure 1. Large scale circulation as observed during (a) the winter (northeast) monsoon, and (b) the summer (southwest) monsoon. (courtesy of W. Düing).

turns south to join the South Equatorial Current (SEC), and the other turns north and joins the NEC.

Above the equatorial region ( $10^{\circ}$  N to  $23^{\circ}$  N) in the Bay of Bengal, the circulation is anticyclonic (clockwise in the northern hemisphere), driven by the northeasterly wind. The western extreme of this circulation is a relatively intense boundary current flowing northward along the coast of India. Between the Andaman and Nicobar Islands and Malaysia, in the Andaman Sea, the drift is southwest, joining the principal branch of the NEC.

During the summer months, when the monsoon is longer and stronger, [Fein, 1987], the southwesterly wind curls around the island of Sri Lanka into the Bay of Bengal. In the western part of the Indian Ocean, the winds drive a broad flow from west to east, the Indian Monsoon Current (IMC). When this current reaches about  $80^{\circ}$  E, it joins the SEC at  $8^{\circ}$  S.

Düing [1970] uses the geostrophic method with the observations from the Indian Ocean Experiment to show the circulation in the Bay of Bengal during the summer is not a simple cyclonic gyre but a more complicated system of cyclonic and anticyclonic eddies on order 100 to 1000 km. At some point in the summer, however, flow in the Bay of Bengal can be described as generally cyclonic throughout.

The model accurately reproduces these flows, in general agreement with the atlases previously discussed. In this

The model accurately reproduces these flows, in general agreement with the atlases previously discussed. In this

presentation the model is first described. Next, a description of the climatology of the winds which force the model is given. Finally, the results of the model are presented, first in terms of general circulation patterns and later in terms of oscillations of certain features.

## 2. MODEL

Isopycnic layered models have proven to be useful in the study of ocean dynamics. The work of *Luther and O'Brien* [1985] and *Luther et al* [1985] demonstrate how a reduced gravity model can correctly simulate the currents of the western Indian Ocean. Further, in *Woodberry et al.* [1989], this model is shown to be equally capable in reproducing the complex current system of the southern Indian Ocean. The success of these efforts gives rise to the numerical model used for this investigation of currents in the Bay of Bengal.

The model employed for this study was developed at the Florida State University by *Jensen* [1990] and is based on the work of Luther and O'Brien. This model, however, is composed of four isopycnal layers. The advantage of a multi-layered model is the ability of studying both surface and subsurface currents. In addition, multiple layers provide greater accuracy in representing low vertical modes.

The layers of this model are assumed to have positive thickness everywhere at all times. In other words, the layers can not merge or surface, and the bottom topography is always in the lowest layer. The vertical modes for the Indian Ocean, given by *Gent et al.* [1983], are used to select the densities and initial layer lowest layer. The vertical modes for the Indian Ocean, given by *Gent et al.* [1983], are used to select the densities and initial layer

thicknesses. The four densities are chosen to be 1023.9, 1026.2, 1027.3 and 1027.9 kg m<sup>-3</sup>. The initial thicknesses of the layers are taken as 200 m for the top layer, 250 m for the second layer, and 400 m for the third.

For this model, horizontal eddy viscosity is based on the velocity field so that a thin layer with large velocities would experience more friction than a thick layer with equivalent transport. The magnitude of the horizontal friction coefficient is taken to be 750 m<sup>2</sup> s<sup>-1</sup>.

Wind forcing at the surface is the only vertical stress that is applied, and it acts as a body force on the upper layer. Forcing due to the gradient in atmospheric pressure is ignored, since when taken in comparison to the wind stress, it is negligible for mesoscale motion. The barotropic modes, which give rise to gravity waves of large phase speed, are removed with the assumption of zero pressure gradient in the lower layer (the reduced gravity approximation).

Following the procedure of *Jensen* [1990], the model equations become, in spherical coordinates,



$$\begin{aligned} \frac{\partial U_j}{\partial t} + \frac{1}{a \cos \theta} \frac{\partial}{\partial \phi} \left( \frac{U_j^2}{H_j} \right) + \frac{1}{a} \frac{\partial}{\partial \theta} \left( \frac{U_j V_j}{H_j} \right) - \frac{2U_j V_j}{a H_j \cot \theta} - f V_j = \\ \frac{-H_j}{\rho_j a \cos \theta} \left[ \frac{\partial p_a}{\partial \phi} + \rho_j g \frac{\partial \eta}{\partial \phi} - g \sum_{i=1}^{j-1} (\rho_j - \rho_i) \frac{\partial H_i}{\partial \phi} \right] + \left( \frac{\tau_j^{\phi, t}}{\rho_j} - \frac{\tau_j^{\phi, b}}{\rho_j} \right) + F^\phi \end{aligned} \quad (1)$$

and

$$\begin{aligned} \frac{\partial V_j}{\partial t} + \frac{1}{a \cos \theta} \frac{\partial}{\partial \phi} \left( \frac{U_j V_j}{H_j} \right) + \frac{1}{a} \frac{\partial}{\partial \theta} \left( \frac{V_j^2}{H_j} \right) + \frac{U_j^2 - V_j^2}{a H_j \cot \theta} + f U_j = \\ \frac{-H_j}{\rho_j a} \left[ \frac{\partial p_a}{\partial \theta} + \rho_j g \frac{\partial \eta}{\partial \theta} - g \sum_{i=1}^{j-1} (\rho_j - \rho_i) \frac{\partial H_i}{\partial \theta} \right] + \left( \frac{\tau_j^{\theta, t}}{\rho_j} - \frac{\tau_j^{\theta, b}}{\rho_j} \right) + F^\theta \end{aligned} \quad (2)$$

where,

$U_j, V_j$  = Zonal and meridional components of vertically integrated volume components for layer  $j$

$H_j$  = Thickness of layer  $j$

$\rho_j$  = Density of layer  $j$

$P_a$  = Atmospheric pressure

$a$  = Radius of the earth

$\phi$  = Longitude

$\theta$  = Latitude

$\theta$  = Latitude

- $f$  = Coriolis parameter  
 $g$  = Gravitational acceleration  
 $\eta$  = Surface displacement  
 $\tau$  = Tangential stress due to vertical friction  
 $F\phi$  = Horizontal friction for U transport, given by

$$A \left[ H_j \nabla^2 \left( \frac{U_j}{H_j} \right) - \frac{1}{a^2 \cos^2 \theta} \left[ U_j (1 - 2 \cos^2 \theta) + 2 \sin \theta H_j \frac{\partial}{\partial \phi} \left( \frac{V_j}{H_j} \right) \right] \right] \quad (3)$$

- $F\theta$  = Horizontal friction for V transport, given by

$$A \left[ H_j \nabla^2 \left( \frac{V_j}{H_j} \right) - \frac{1}{a^2 \cos^2 \theta} \left[ V_j (1 - 2 \cos^2 \theta) + 2 \sin \theta H_j \frac{\partial}{\partial \phi} \left( \frac{U_j}{H_j} \right) \right] \right] \quad (4)$$

The continuity equation is

$$\frac{\partial H_j}{\partial t} + \frac{1}{a \cos \theta} \left[ \frac{\partial U_j}{\partial \phi} + \frac{\partial}{\partial \theta} (V_j \cos \theta) \right] = w_e \quad (5)$$

where,

$w_e$  = Turbulent entrainment velocity between first and

$w_e$  = <sup>second layers</sup> Turbulent entrainment velocity between first and

second layers

This entrainment term is included to prevent the interface between the top two layers from surfacing, that is, the upper layer thickness cannot go to zero. This term is positive in the case when the upper layer thickness becomes less than a prescribed value,  $H_{\min}$ , and negative for the same case in the second layer and is given by

$$w_e = \begin{cases} \frac{(H_1 - H_{\min})^2}{\tau_e H_{\min}} & H_1 \leq H_{\min} \\ 0 & H_1 > H_{\min} \end{cases} \quad (6)$$

For the bottom two layers this term is set to zero. The effect of this entrainment on the upper layer momentum balance is neglected. Incorporating this entrainment velocity only in the continuity equation represents turbulent entrainment where entrained water into the upper layer has zero velocity and is warmed instantaneously to the upper layer density. For this particular study, however, this adjustment is rarely active. The

value for  $H_{\min}$  is taken to be 60 m and the time constant  $\tau_e$  is 1.2 hours.

The boundary conditions for this set of equations are given in two parts. First, for closed boundaries, i.e. land, the no-slip condition is incorporated. At coastal points, therefore, both components of the transport are set to zero. Next, for open boundaries, a Sommerfield radiation condition is applied. The solution at the boundary is first separated into its vertical modes, and the radiation condition is applied to each mode separately. The resulting current components for the boundary are computed as the sum of these vertical modes.

The only forcing is the applied wind stress. The wind forcing is based on wind stress values taken from a climatological monthly mean data set prepared by *Hellerman and Rosenstein* [1983]. A pseudo-stress is formed by dividing these data values by the product of an average drag coefficient and an air density. For this study a constant drag coefficient of 0.0015 and an air density of  $1.2 \text{ kg m}^{-3}$  are applied. A bicubic spline is then used to interpolate the data from their two degree resolution down to the model resolution.

The domain of the model is from  $25.1^\circ \text{ S}$  to  $26.1^\circ \text{ N}$  and from  $34.8^\circ \text{ E}$  to  $119.6^\circ \text{ E}$ . It should be noted that the model domain is much larger than the domain of interest for this study. Results are  $34.8^\circ \text{ E}$  to  $119.6^\circ \text{ E}$ . It should be noted that the model domain is much larger than the domain of interest for this study. Results are

investigated only in a small section of the total model domain. The open boundaries for the model are along the 25° S parallel and along the 119° E meridian between Australia and Indonesia. Figure 2 shows the domain of the entire model, with a border outlining the region of interest for this study.

The land values are given by the 200 meter isobath. It is for this reason that shallow areas, which pose a significant impedance to flow, such as the channel between India and Sri Lanka, appear as land. Additionally, the two island chains, Nicobar and Andaman, appear as solid stretches of land.

With these boundary conditions established, the equations are discretized, using a resolution of one-tenth of a degree in both horizontal directions. This was done, for the spatial derivatives, using the Arakawa C-grid, which is a mass and energy conserving scheme. The time integration was performed using an explicit leap-frog scheme with a forward Euler scheme applied every 99 time steps to remove the computational mode inherent to the leap-frog method. The Laplacian friction term is computed with a Dufort Frankel implicit scheme [O'Brien, 1986] for computational convenience.

The model is spun up from rest, with a time step of twenty minutes, by repeatedly applying the annual wind stress cycle. After ten years a quasi-periodic solution is obtained. The

After ten years a quasi-periodic solution is obtained. The

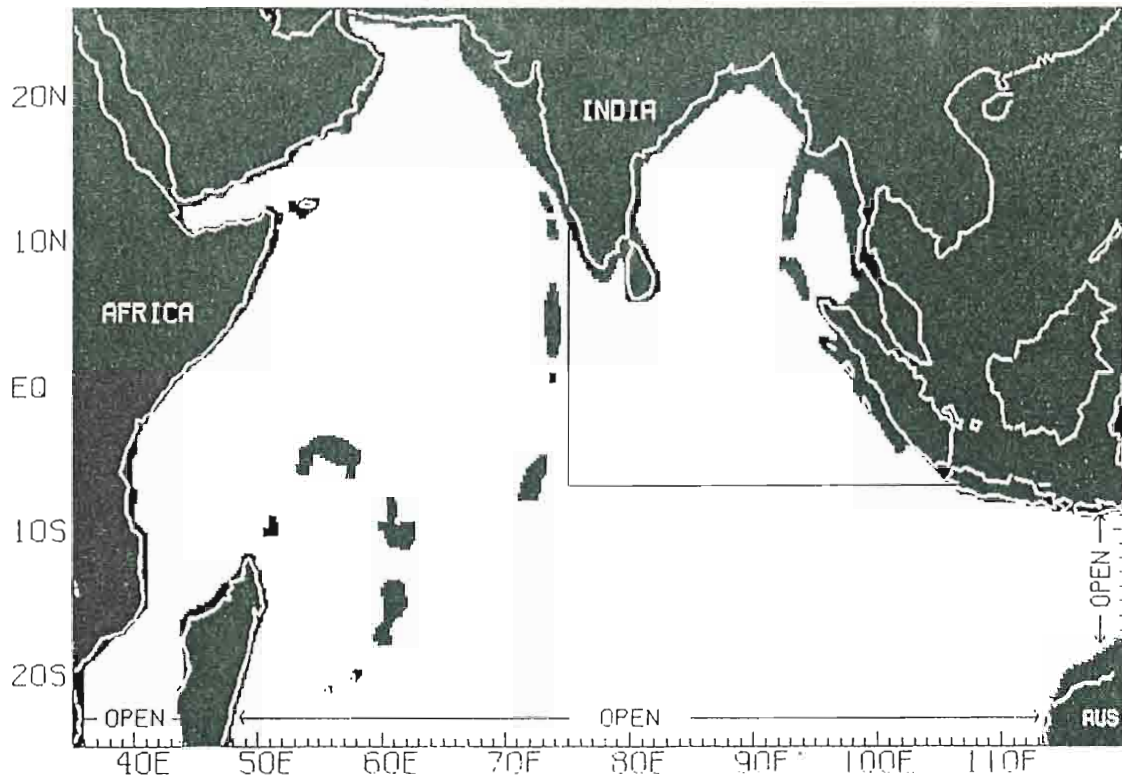


Figure 2. Model domain. The 200 m isobath is used for land boundaries, and the open boundaries are labeled. The border in the northern part of the domain indicates the particular region investigated in this study. The border in the northern part of the domain indicates the particular region investigated in this study.

computer results are retained as fields of currents and layer thickness every six days.

### 3. WINDS

Monsoon regions are considered those which experience the seasonal reversal in winds during the year. The Indian Ocean, characterized by large season to season variations due to the Asian Monsoons, is one such region. In the area of the Bay Bengal the winds are southwesterly during the northern summer months and switch to northeasterly during the months of the northern winter. The primary driving force for this oscillation in wind patterns is the differential heating between land and water.

The northeasterly winds of the winter monsoon are caused by a high pressure cell which forms over the Asian mainland due to the rapid cooling there. With the warmer summer climate, the Asian mainland begins to warm. This occurs faster than the warming of the ocean water, and a low pressure is formed over the land. This combines with a high pressure formed over the Mascarene Basin and the southeast trades producing strong southwesterly winds (the summer monsoon system) [*Hastenrath*, 1985].

Figure 3 is a schematic description of the two monsoon systems. A major difference between the two systems is the geometry of the underlying surface. In the summer monsoon the general ascent and rainfall occur over warm land areas while the geometry of the underlying surface. In the summer monsoon the general ascent and rainfall occur over warm land areas while the



## SUMMER MONSOON

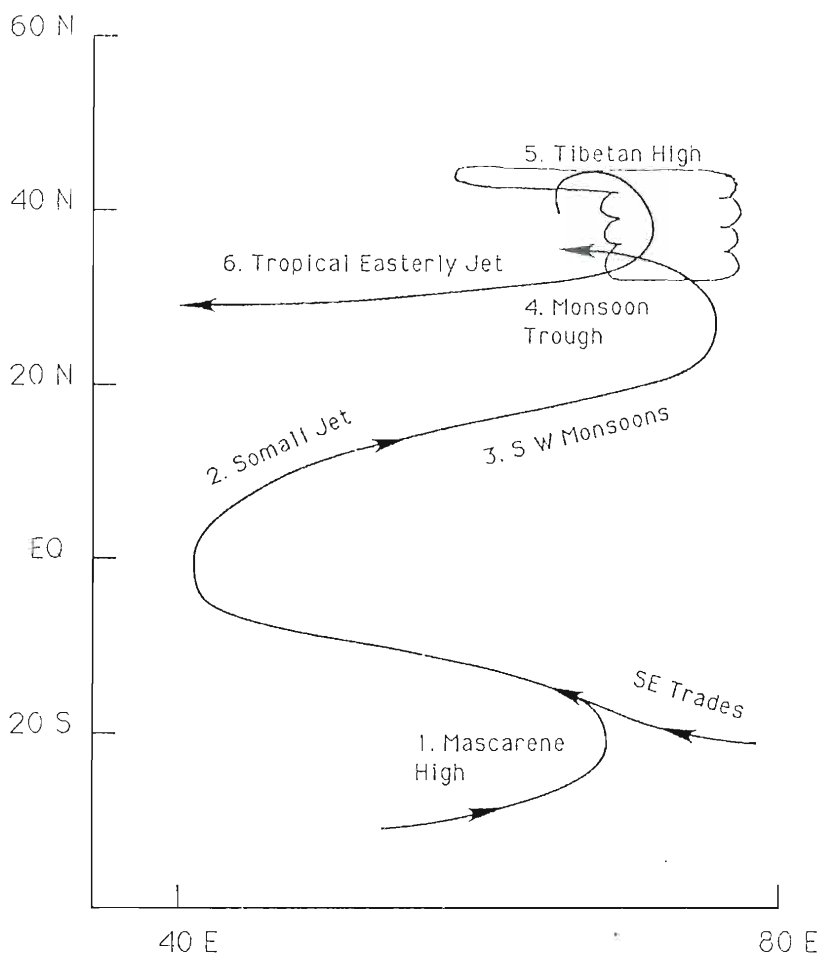


Figure 3. Schematic representation of monsoon system. The six components of the monsoon may be equated as: 1) the Mascarene high of summer and the Siberian high of winter; 2) the cross equatorial low level jet over East Africa during summer and the lower tropospheric surges during winter; 3) the summer monsoon rainfall and cloud cover over northern India and its counterpart near southern Malaysia and Indonesia during winter; 4) the summer monsoon trough over northern India and the winter monsoon trough over Indonesia; 5) the upper tropospheric Tibetan high of summer and the upper tropospheric Western Pacific high of winter; 6) the tropical easterly jet stream during summer and the subtropical jet stream of winter (courtesy of T. N. Krishnamurti).

or winter, 6) the tropical easterly jet stream during summer and the subtropical jet stream of winter (courtesy of T. N. Krishnamurti).

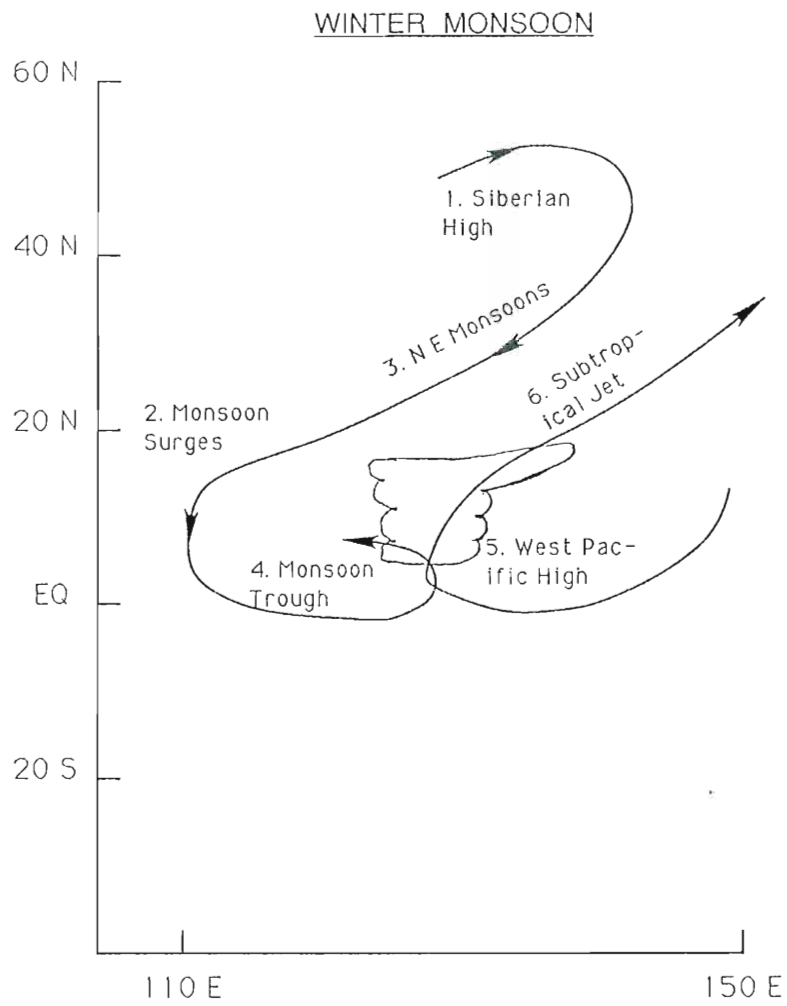


Figure 2. Continued.

Figure 3. Continued.

descent occurs over the southern Indian ocean. During the winter monsoon, the general ascent and rainfall occur over a marine environment while the descent occurs over the land areas of eastern Asia. This implies that the main driving mechanism of the summer monsoons is the shortwave radiative warming over land areas, while the winter monsoon is driven by longwave cooling over the land areas [*Fein*, 1987].

The wind patterns associated with the monsoon climate are compiled in the form of wind stress into a data set by *Hellerman and Rosentien* [1983]. The model was forced by this climatological wind data set. This set was obtained by processing surface observations for approximately one hundred years (1870-1976) and calculating monthly norms and standard deviations of the eastward and northward components of wind stress at standard anemometer height (ten meters).

Figures 4a and 4b represent the wind conditions of January and July (the contours shown are the pseudostress values used to force the model). These are representative of the extreme conditions of the winter and summer monsoons, respectively. The months of April and October, shown in Figures 4c and 4d, demonstrate the transition period between the monsoon seasons. A more complete picture of the atmospheric conditions of the Indian Ocean can be found in the atlas by *Hastenrath and Lamb* [1979].

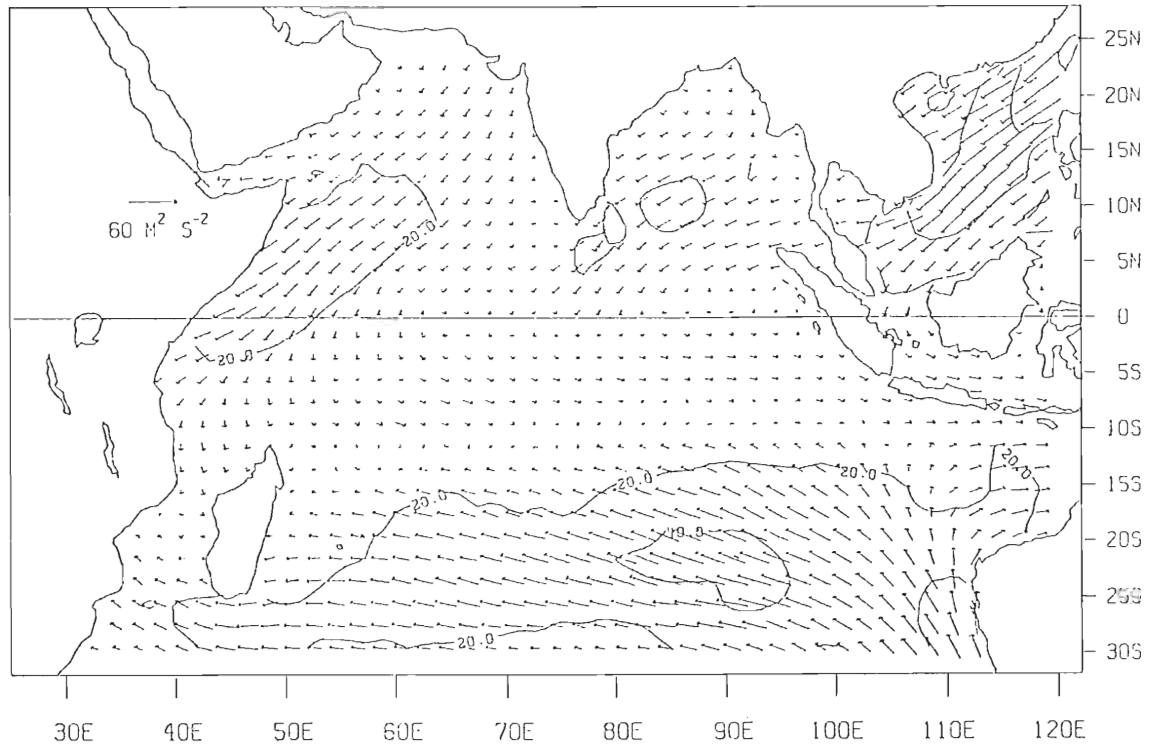


Figure 4a. Monthly mean wind field for January. The vectors give direction for the wind field while the contours give the pseudostress magnitude. The contour interval is  $20 \text{ m}^2 \text{ s}^{-2}$ . This pattern is representative of the winter monsoon. The winds come down from the continent in a southwestward direction. They begin to weaken at the equator and turn eastward. Below the equator the atmospheric flow is predominantly to the east. The maximum wind velocities are found along  $6^\circ \text{ N}$ . The minimum is centered about the equator.

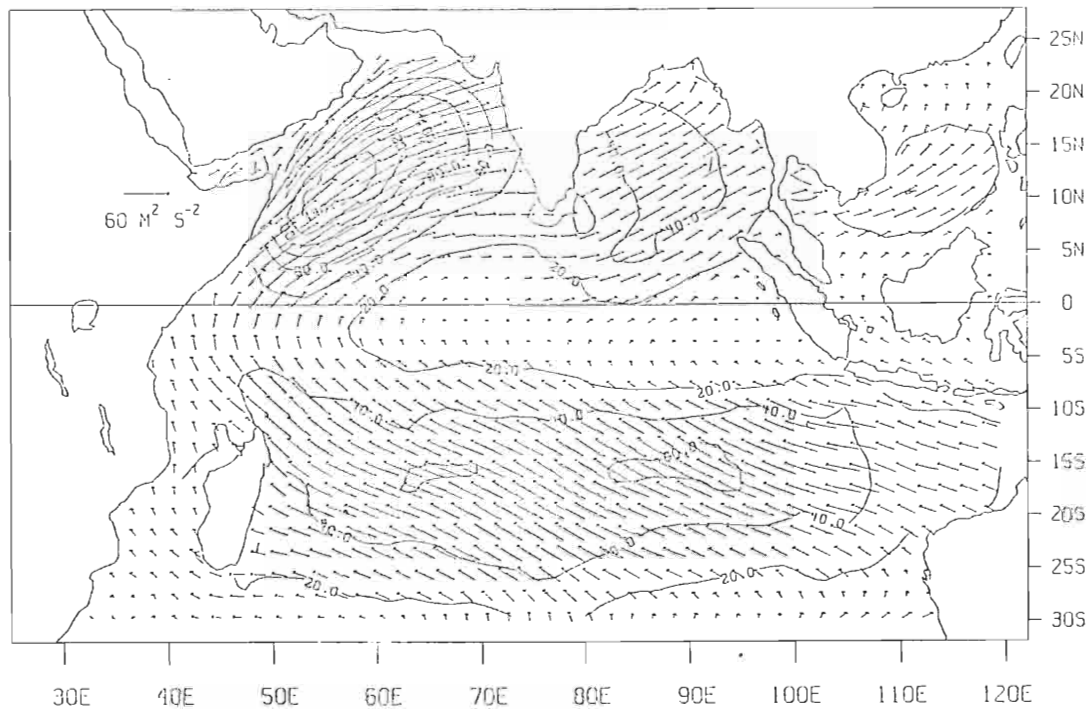


Figure 4b. Monthly mean wind field for July. The contour interval is the same as Figure 4a, and this case typifies the summer monsoon. Winds in the Bay of Bengal are strictly towards the northeast, while below the equator they are more northward in direction. The maximum for this time of year occurs in the center of the bay, and the minimum has moved to just south of the equator.

QUESTION: The maximum for this time of year occurs in the center of the bay, and the minimum has moved to just south of the equator.

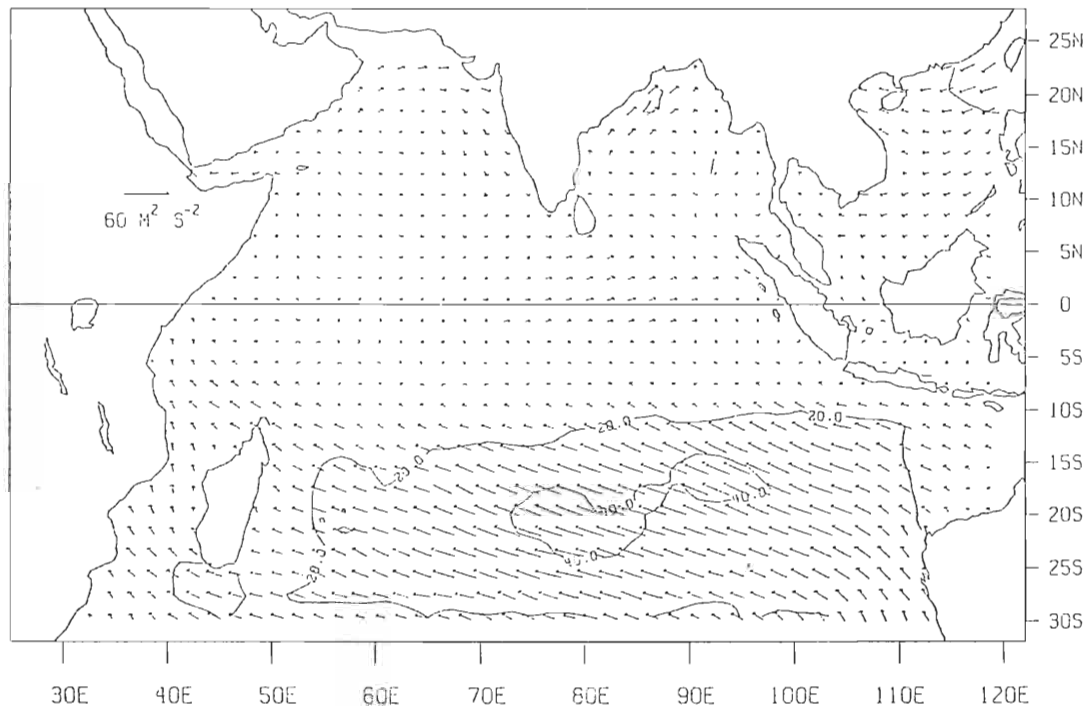


Figure 4c. Monthly mean wind field for April. Same as for Figure 4a except this is the time of transition from the winter monsoon to the summer. An anticyclone has developed over the bay, fed by eastward flowing winds along the equator. The greatest wind speeds are found along the Indian mainland.

the summer. An anucyclone nas developed over the bay, fed by eastward flowing winds along the equator. The greatest wind speeds are found along the Indian mainland.

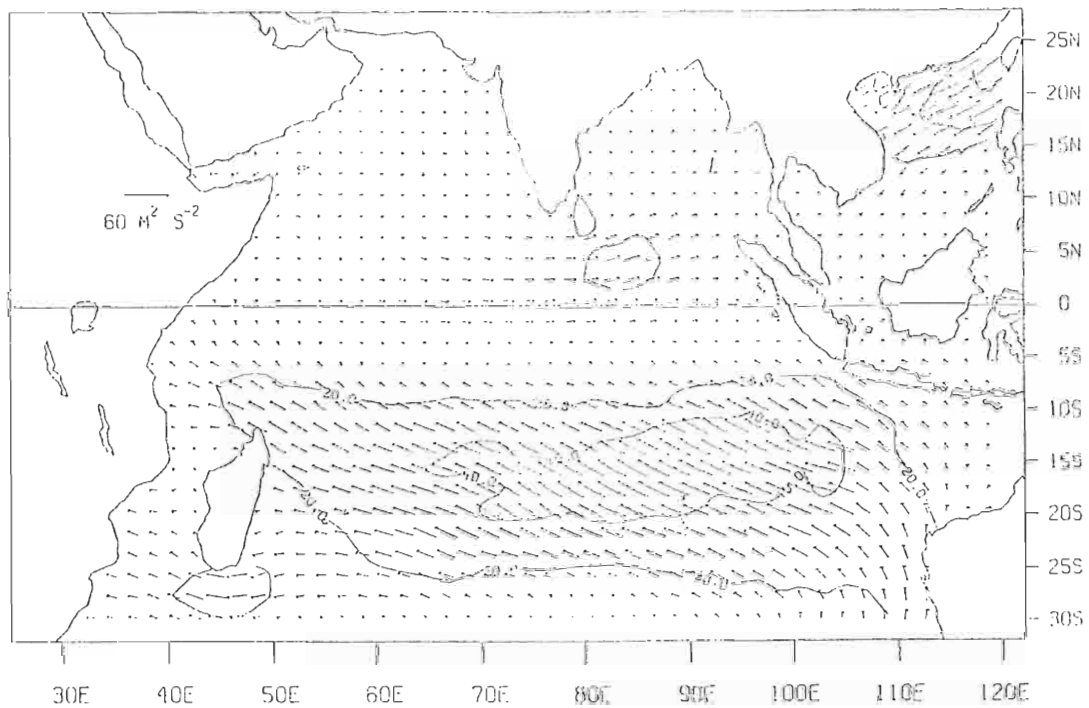


Figure 4d. Monthly mean wind field for October. Same contour values as Figure 4a except it is the transition period from the summer monsoon to the winter. Flow is eastward along the equator, turning northward at land. The velocities are somewhat weaker with the maximum occurring just above the equator.

During the northern hemisphere winter monsoon months of November to February, the winds flow from the high pressure area over the Asian continent into the Bay of Bengal in a southwestward direction. These winds reach a maximum of about  $6 \text{ m s}^{-1}$  off the east coast of India during the month of December. In the beginning stages of the winter monsoon (November) the winds in the bay itself have a strong westward component down to approximately  $7^\circ \text{ N}$ . Below  $7^\circ \text{ N}$ , down to approximately  $5^\circ \text{ S}$ , the winds are very zonal toward the east. During winter, therefore,  $7^\circ \text{ N}$  represents a line of cyclonic wind shear. This wind pattern moves south of the equator as the season progresses.

This pattern is manifest as region of large positive wind stress curl in early winter over the Bay of Bengal, down to about  $5^\circ \text{ N}$ . This region of positive wind stress curl moves south as a band between  $10^\circ \text{ N}$  and the equator, bounded to the north and south by regions of negative wind stress curl, during the northern spring months.

During March and April the winter monsoon begins the transition to the summer monsoon. Anticyclonic winds develop over the bay and, in conjunction with the weak maximum in the pressure field, bring flow with a southerly component to the western and northern shores of the bay. During March flow from about  $10^\circ \text{ N}$  down to  $5^\circ \text{ N}$  is mainly toward the west while from the equator to about  $10^\circ \text{ S}$  it is toward the east. This pattern about  $10^\circ \text{ N}$  down to  $5^\circ \text{ N}$  is mainly toward the west while from the equator to about  $10^\circ \text{ S}$  it is toward the east. This pattern



breaks down with the full arrival of the summer monsoon in July. By May the winds are predominantly southwesterly, originating in the southern hemisphere and sweeping through the Bay of Bengal. At the peak of the summer monsoon in July, the maximum wind speeds are found over the center of the bay and are of order  $10 \text{ m s}^{-1}$ .

The summer wind stress curl is somewhat different than that seen in winter. The band of positive wind stress curl is much more narrow, extending from about  $5^\circ \text{ N}$  to  $15^\circ \text{ N}$ . In addition the patch of positive curl runs along the coast to the extreme north of the bay rather than running in a zonal direction. The maximum values appear off the coast of Sri Lanka.

#### 4. REGIONAL CIRCULATION

The large scale circulation in the northern Indian Ocean can be described in three parts. First, there is a large gyre system which develops in the Bay of Bengal, the recirculation portion of which is a western boundary current along the east coast of India [Legeckis, 1987]. The model simulates only wind driven flow, but several factors could determine the circulation in this region. It has been suggested that the river systems of India contribute in a small way to the circulation in the Bay of Bengal [Somayajulu *et al.*, 1987]. One large system is the Ganges which empties into the northern end of the bay. In addition, the severe weather associated with the monsoon affects circulation in the form of tide surges and fresh water input [Johns *et al.*, 1985].

Another component of the circulation in the northern Indian Ocean is the flow into and around the Andaman Sea, bounded by Malaysia in the east and the Nicobar and Andaman Island chains in the west. It could be expected that discrepancies between the model and measured results would be greatest in this region due to the geometry of the model. The model cannot produce flow through the Malacca Strait, since it is less deep than the 200 meter depth contour that the model uses as land (closed boundary). Data records indicate, however, that significant flow meter depth contour that the model uses as land (closed boundary). Data records indicate, however, that significant flow

does travel from the South China Sea into the Andaman Sea through this straight [Cutler and Swallow, 1984]. Similarly, the two island chains are treated by the model as single areas of land, only allowing flow between the two (through the Ten Degree Channel) and between Sumatra and Greater Nicobar Island (through the Great Channel). The model, therefore, treats the Andaman Basin as more of an enclosed area than actually exists.

The final components of the flow field in this region are the equatorial currents. These currents are the northern and southern extremes of gyres centered near the equator [Molinari *et al.*, 1990]. The northern most current is the North Equatorial Current (NEC). It flows toward the west during northern winter, between  $8^{\circ}$  N and the equator [Piccard and Emery, 1982]. Below this current, from the equator to  $8^{\circ}$  S, is the eastward flowing Equatorial Counter Current (ECC). During the summer monsoon, the NEC reverses direction, joins the ECC, and forms the Indian Monsoon Current (IMC) [Molinari *et al.*, 1990]. In addition, an equatorial jet, explained by O'Brien and Hurlbert [1974], is formed during the monsoon transition periods (spring and fall) [Wyrtki, 1973]. This rapid, eastward flowing current is centered about the equator. Further south is the South Equatorial Current (SEC). The SEC flows from east to west all year, from about  $15^{\circ}$  S up to the ECC. While it does not change direction during the year, it does intensify in the northern summer months (May to September).  
does not change direction during the year, it does intensify in the northern summer months (May to September).

In addition to these surface currents, there is also a subsurface current, the Equatorial Undercurrent (EUC) [Cane, 1980]. It is found east of  $60^\circ$  E during the Northern Winter. It is weaker than its counterparts in the Pacific and Atlantic Oceans, and during the Northern Summer, when equatorial flow is to the east, it is not evident [Piccard and Emery, 1982].

In this section, these features are examined using the results of the multi-layered, wind driven model. Whenever possible, comparisons to observed data are made. The large scale features previously mentioned are, in fact, well represented by the model. Figures 5a through 5f show the results of the model at six times during the year. The upper layer thickness, plotted using a color scale, gives an indication of the upper 200 meters of the ocean. The current velocity is shown as vectors, with magnitude relative to the arrow length and direction given by the arrow orientation. Speeds less than  $0.010 \text{ m s}^{-1}$  are not displayed and speeds more than  $0.100 \text{ m s}^{-1}$  are truncated.

Second layer topographies are shown in Figures 6a through 6f. The field in this case represents the distance from the surface to the interface between the second and the third layers of the model. The velocity field is presented the same way as for the upper layer.

The features of both the surface and subsurface circulation can be readily identified from these figures. To get a more

The features of both the surface and subsurface circulation can be readily identified from these figures. To get a more

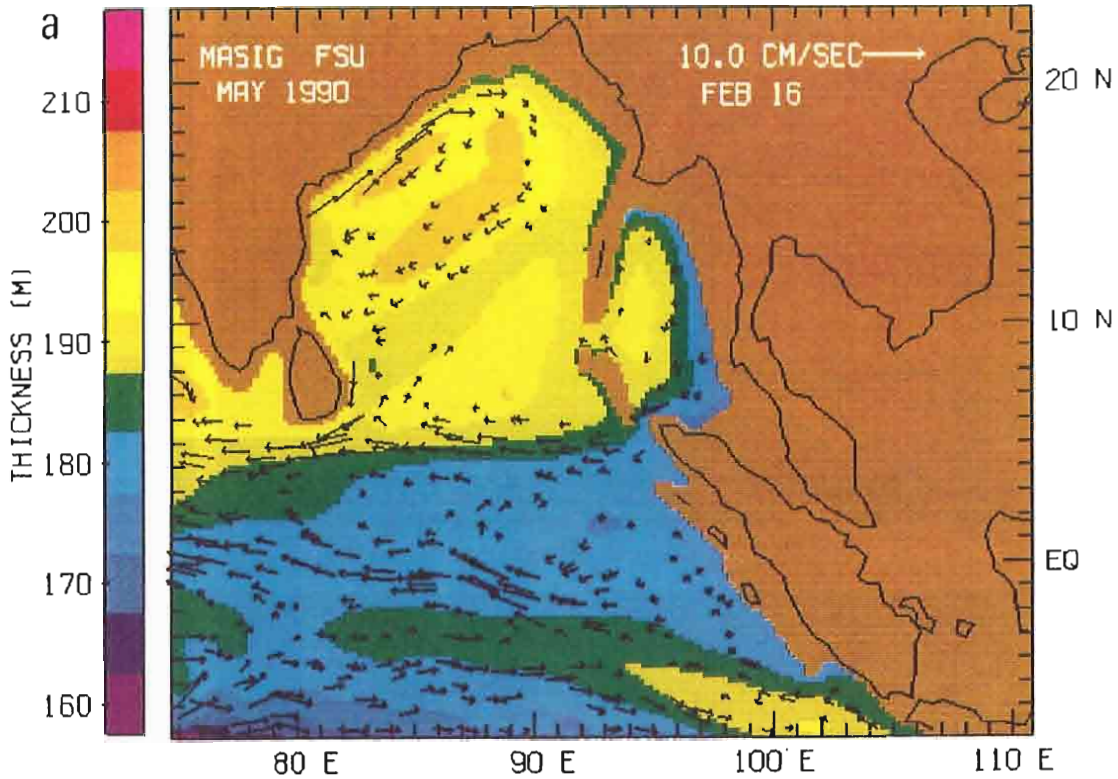
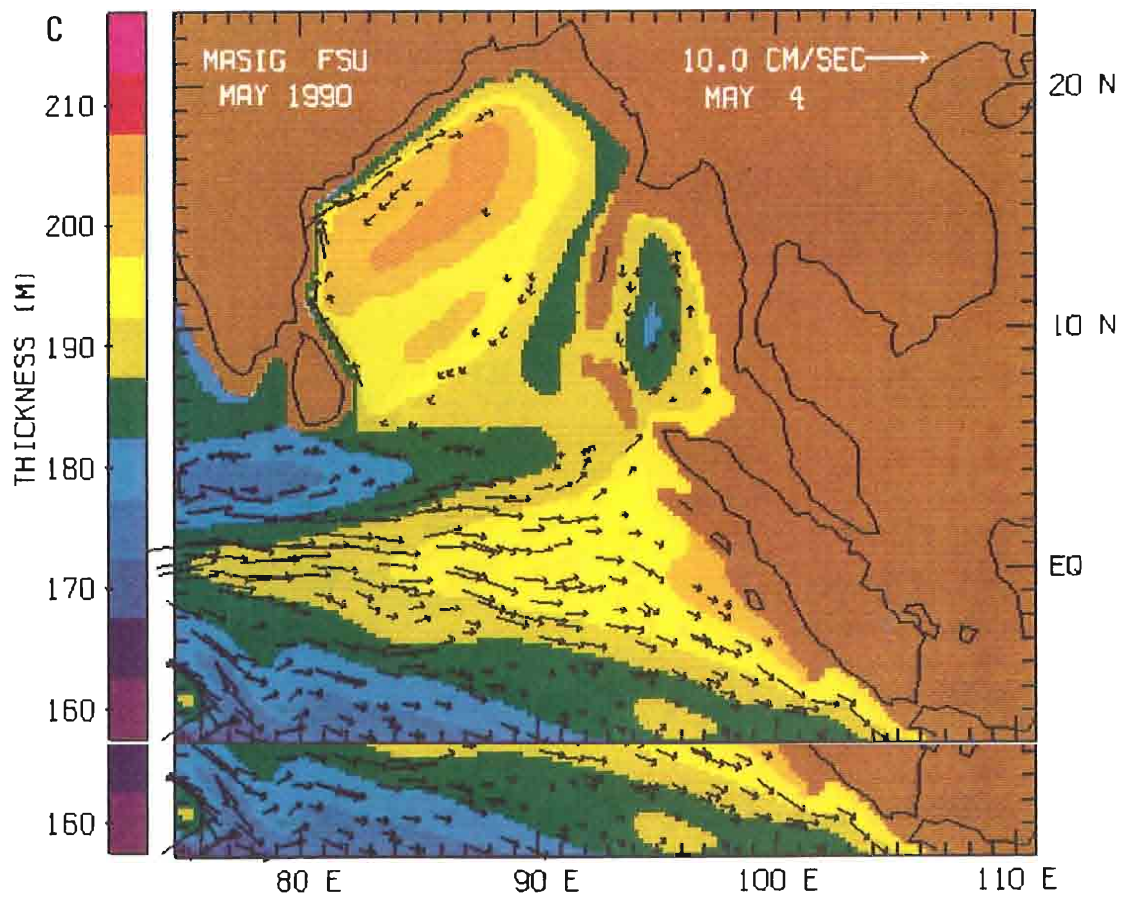
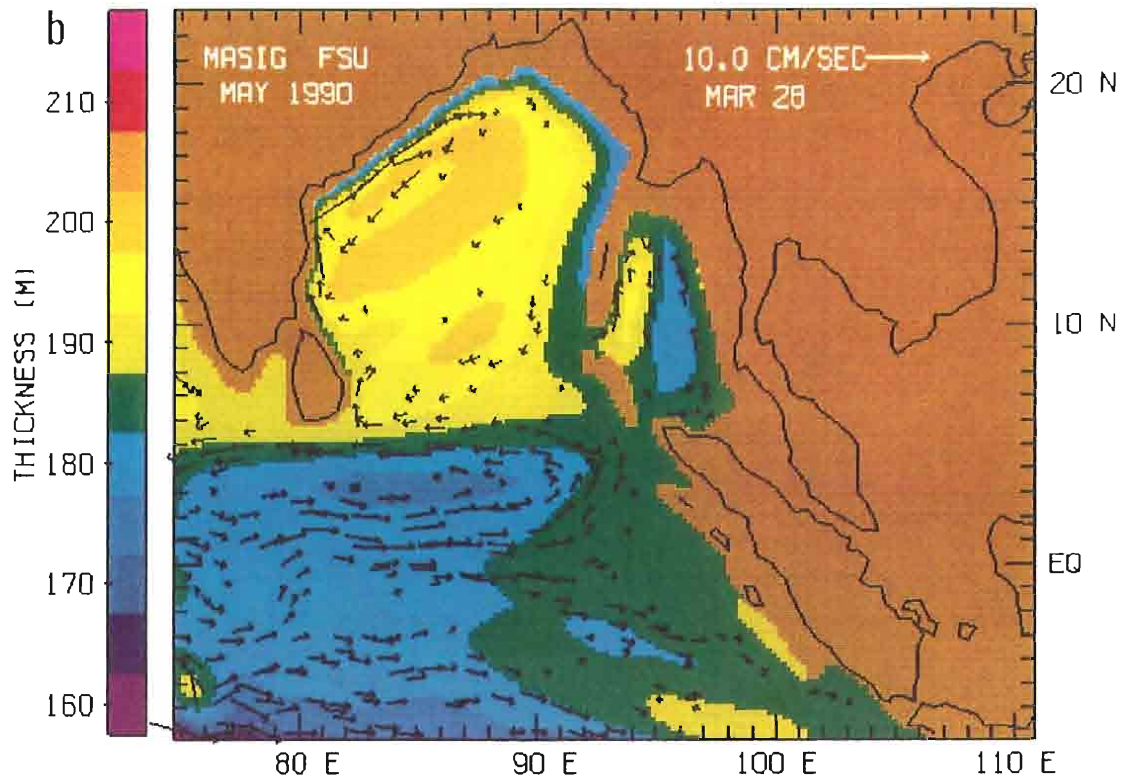
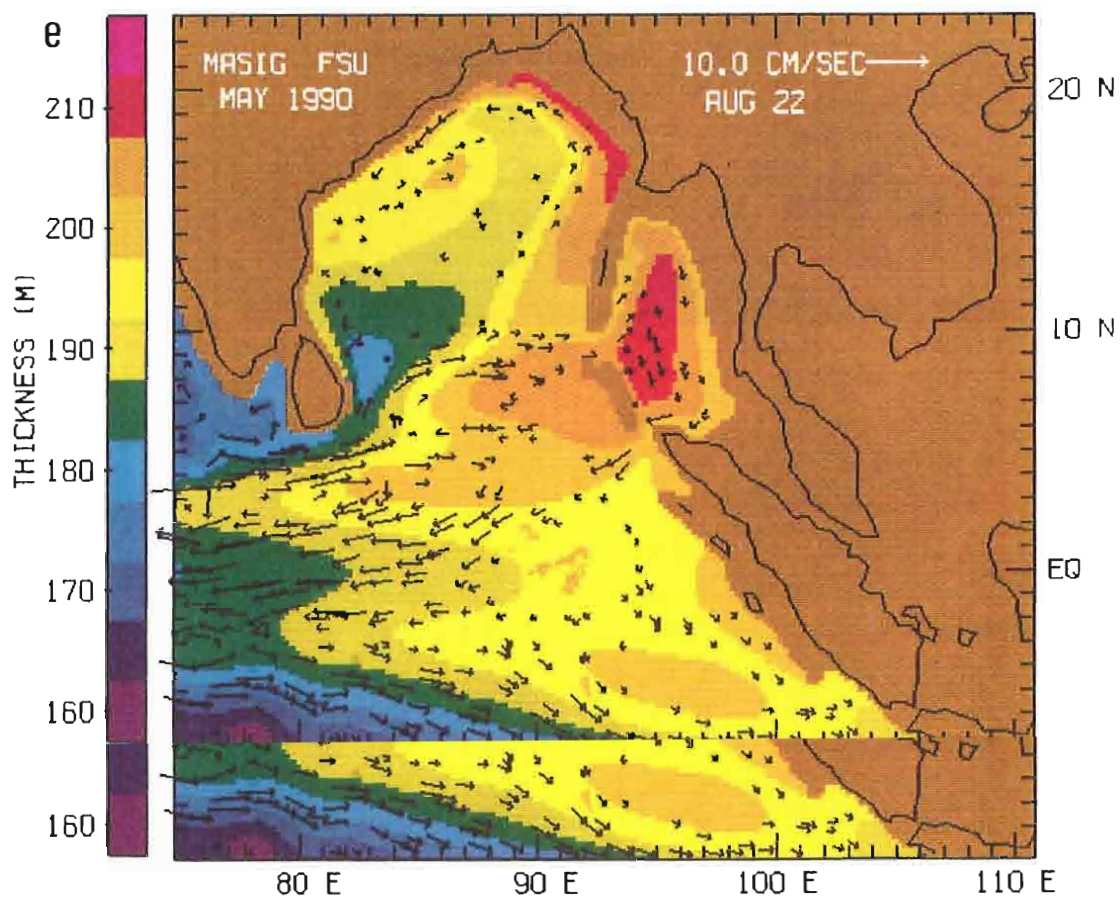
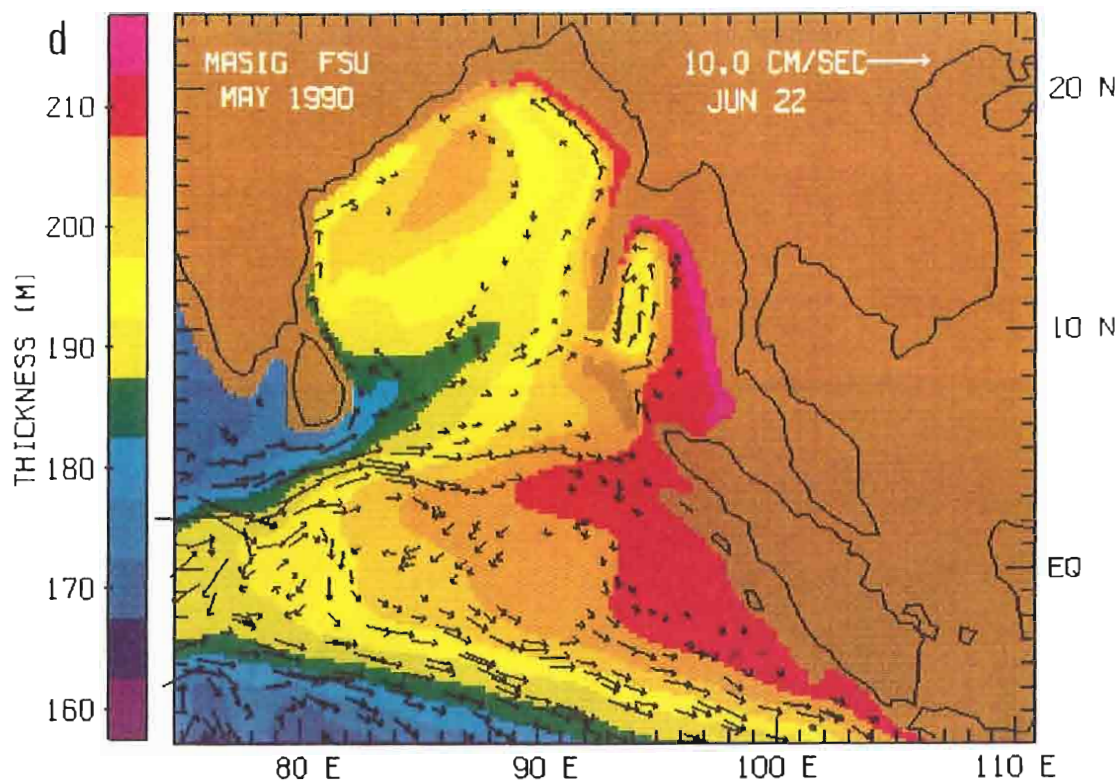
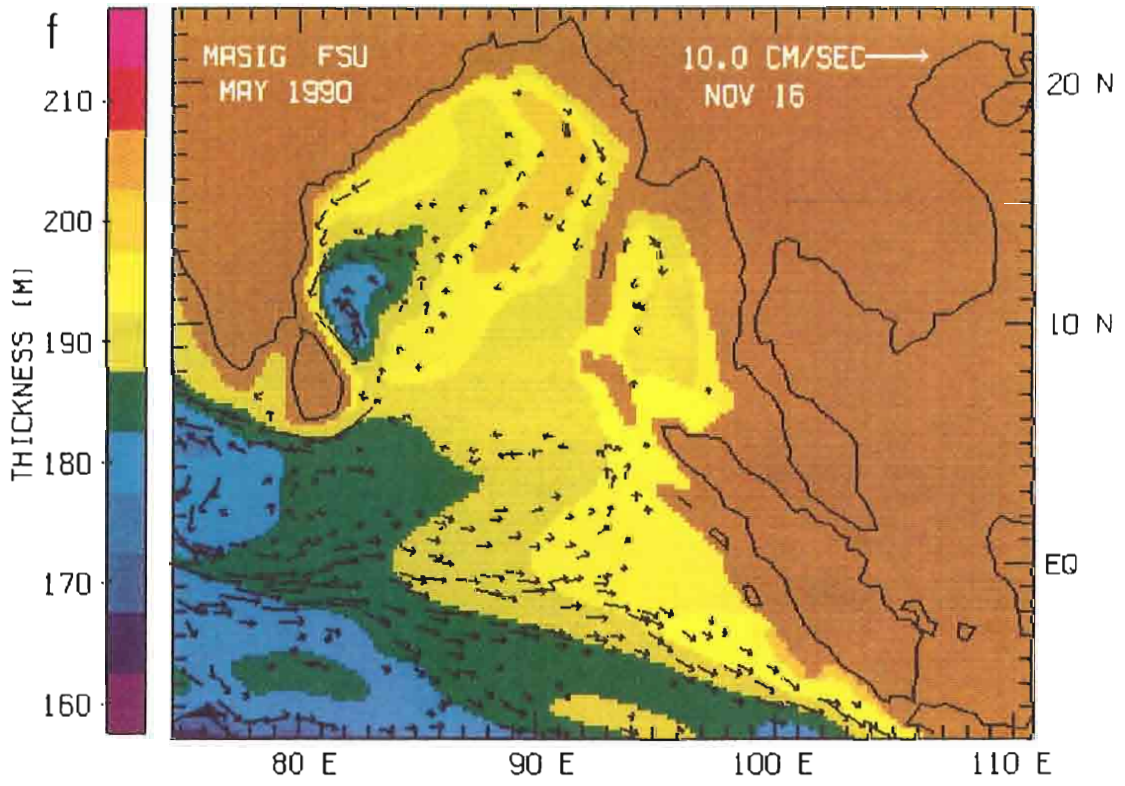


Figure 5. Model results for the surface layer. (a) February. (b) March. (c) May. (d) June. (e) August. (f) November. The thickness of the upper layer is represented by the color scale (in meters), and it reflects dynamic topography. The currents in the surface layer are given by the vectors. The major features of the circulation are the large circular flow in the Bay of Bengal, flow into and around the Andaman Sea, and the equatorial currents. surface layer are given by the vectors. The major features of the circulation are the large circular flow in the Bay of Bengal, flow into and around the Andaman Sea, and the equatorial currents.









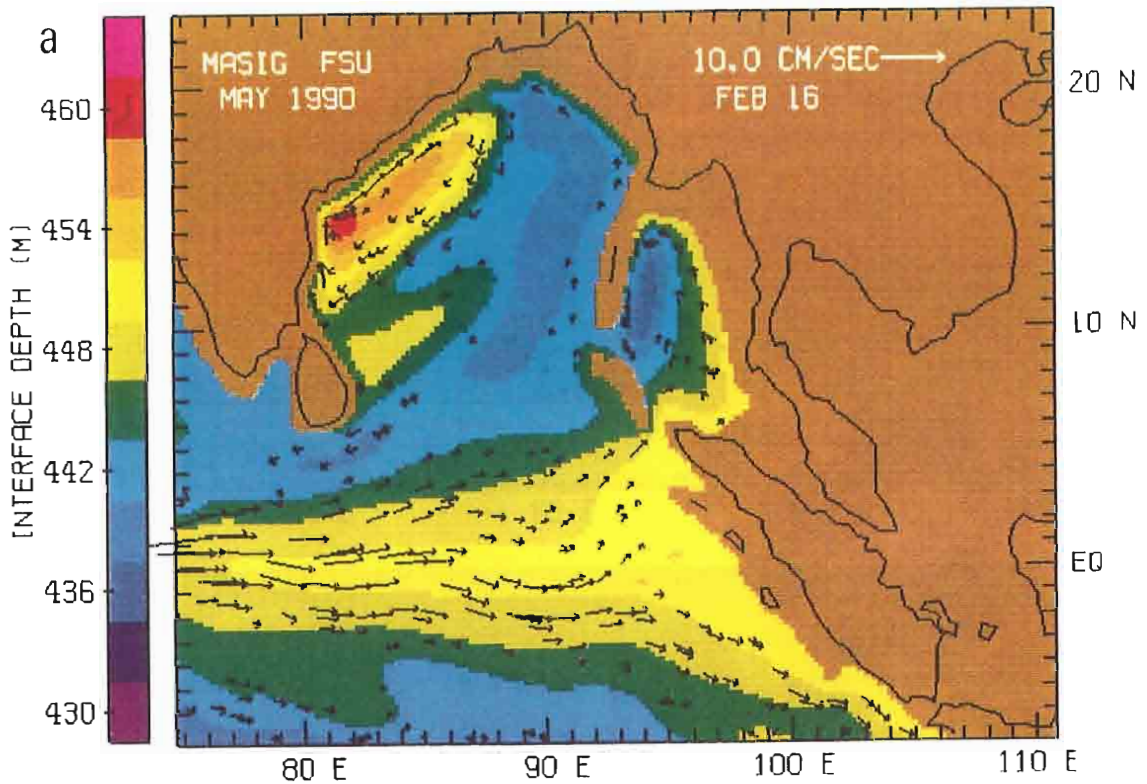
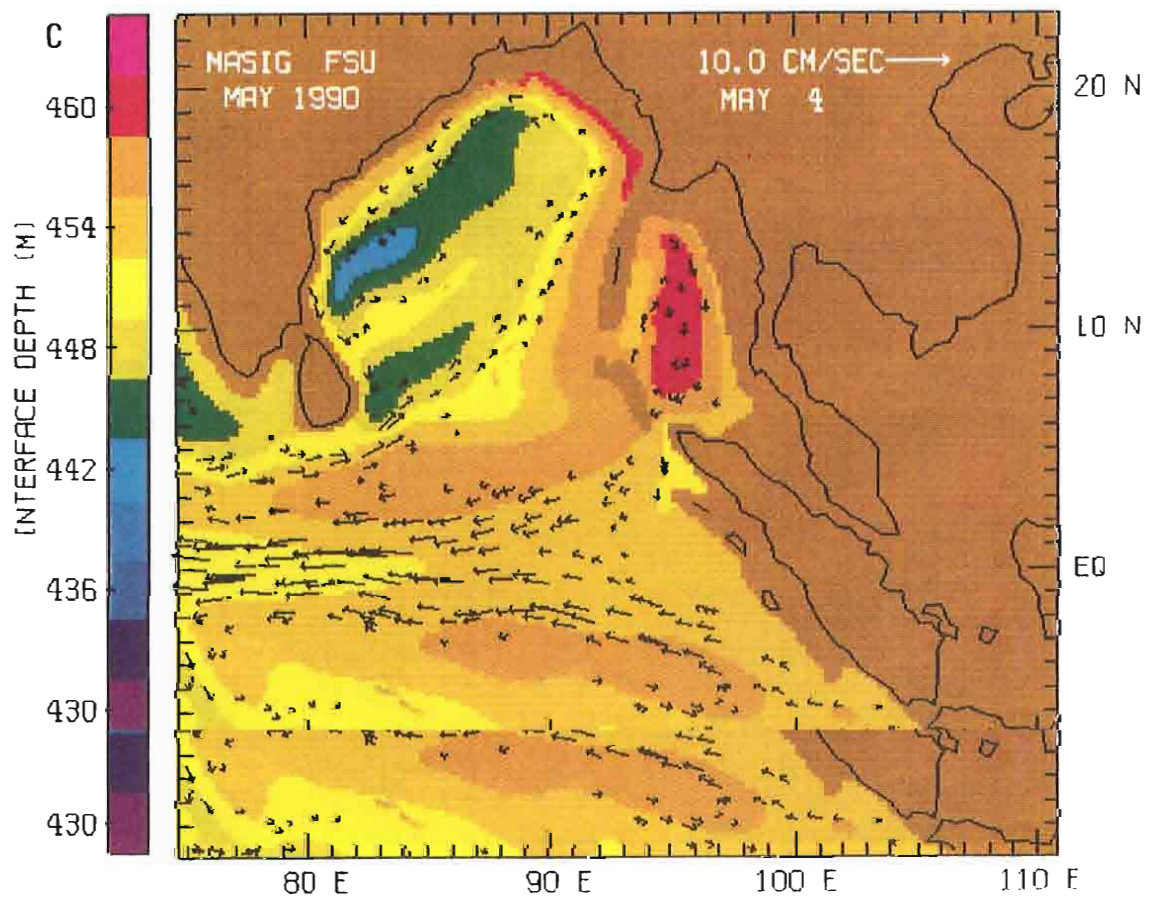
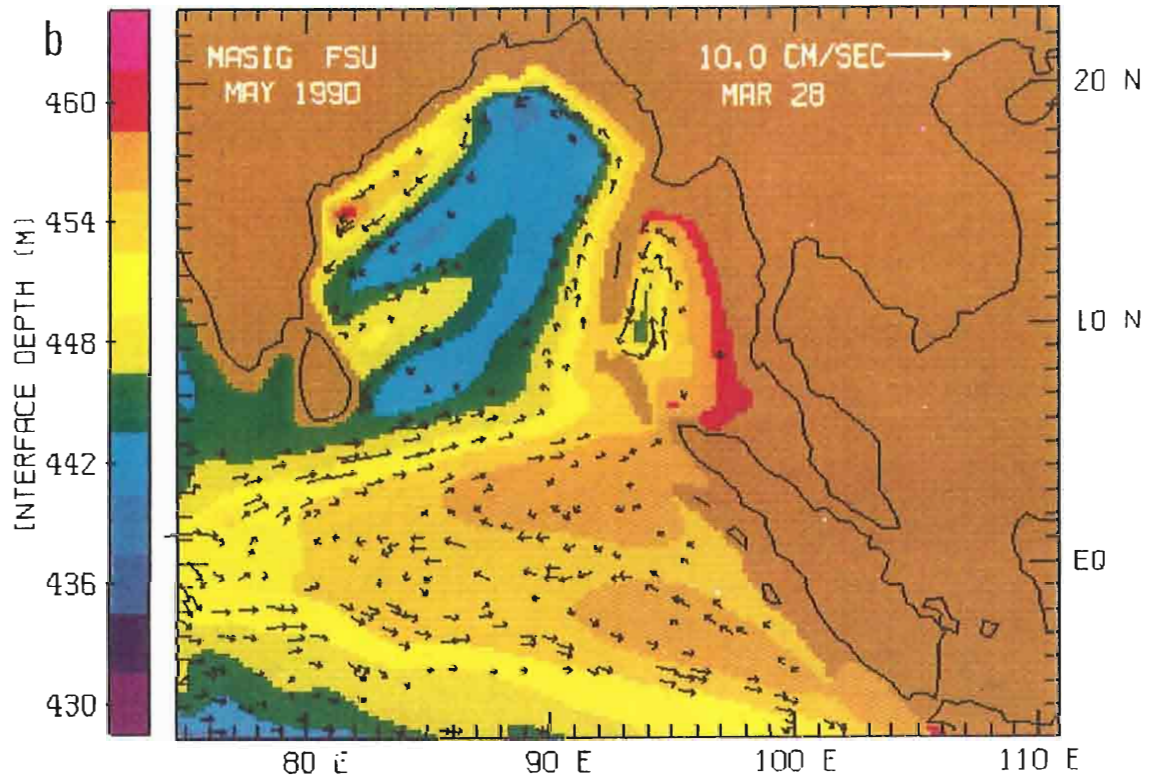
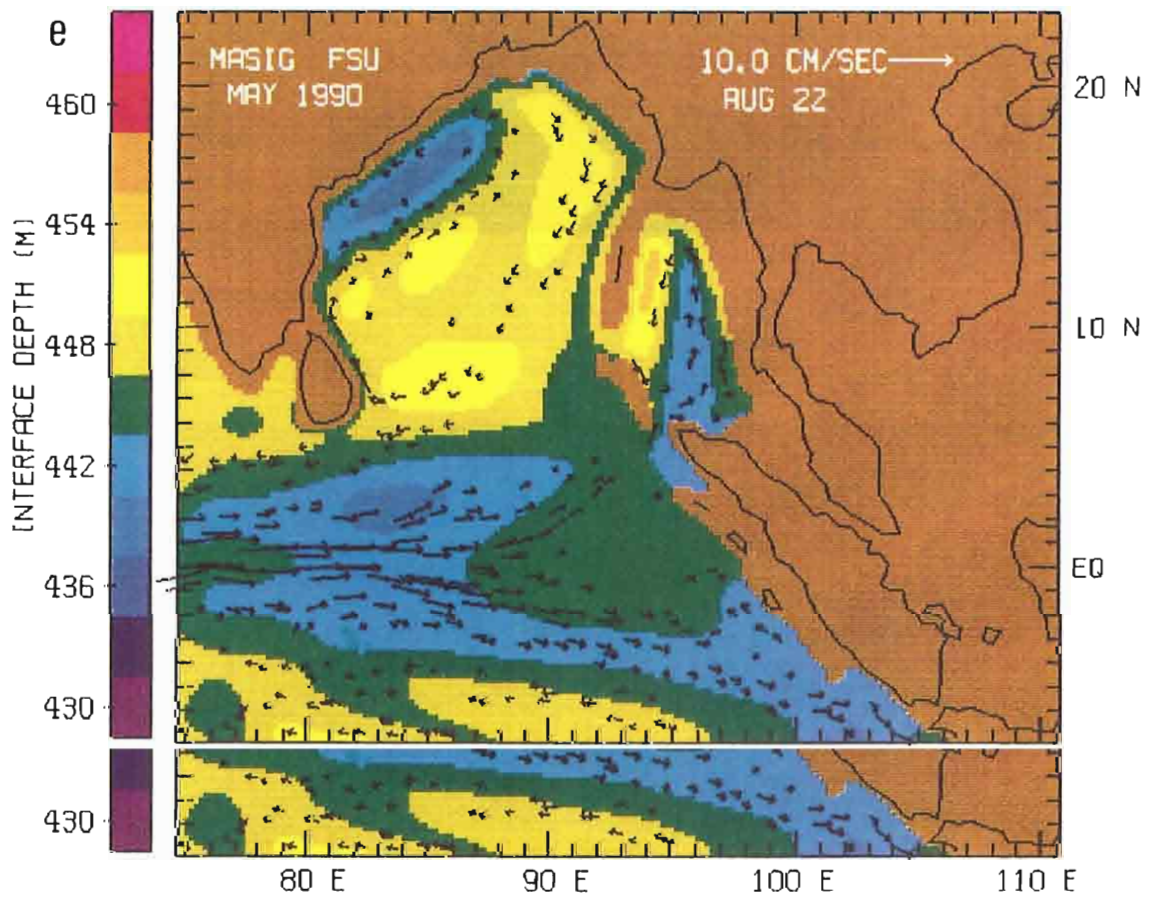
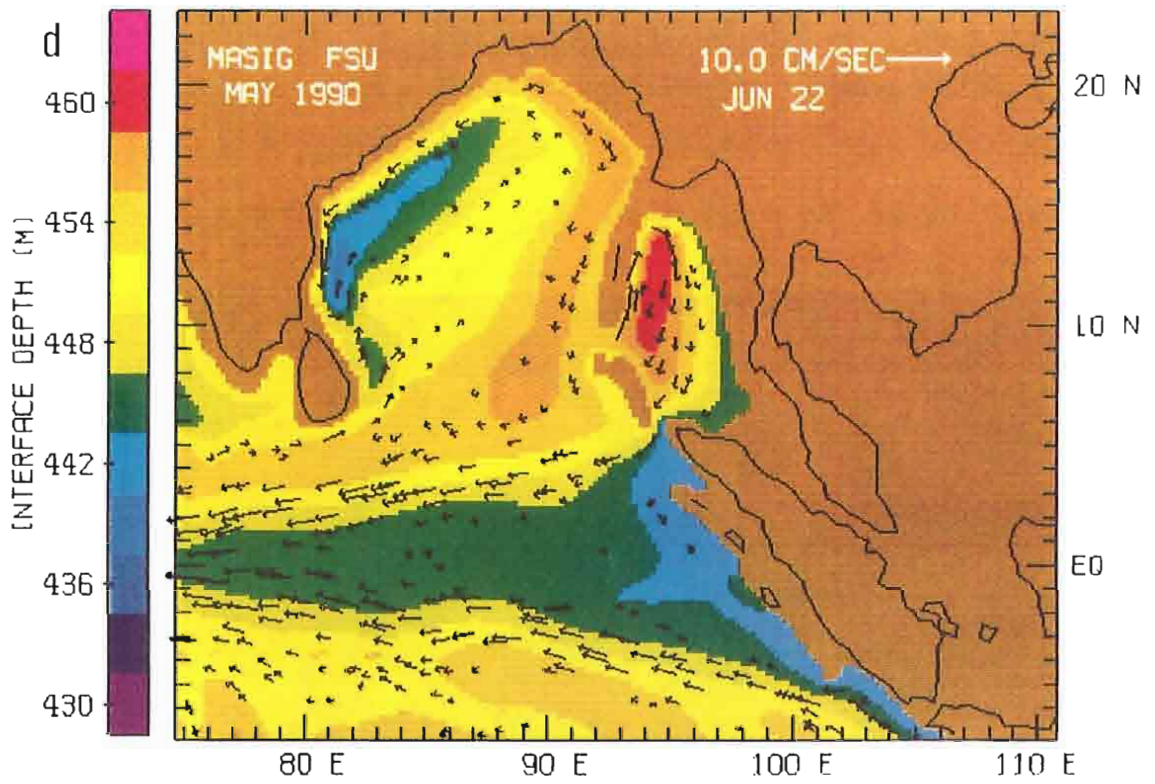
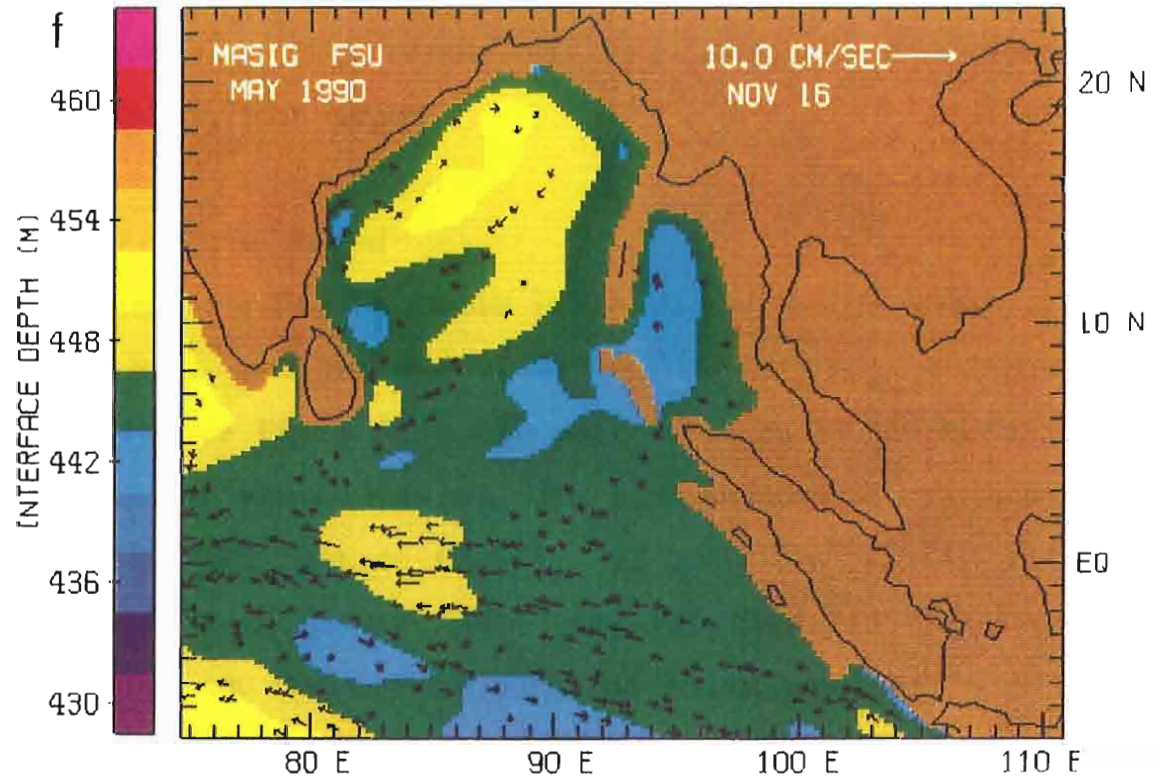


Figure 6. Model results for the second layer. (a) February. (b) March. (c) May. (d) June. (e) August. (f) November. The months are the same as in the case of the surface layer for comparison. The thickness represented by the color scale is the depth of the interface between the second and third layers. are the same as in the case of the surface layer for comparison. The thickness represented by the color scale is the depth of the interface between the second and third layers.







quantitative idea of the flow, transports were computed at certain cross sections using the model data. Figure 7 shows the locations where the calculations of mass transport were made. In the following sections each part of the circulation previously outlined is described. The results of the transport computations are presented as they apply.

#### 4.1 *The Bay of Bengal*

Examining first the results in the Bay of Bengal reveals a large anticyclonic gyre centered at  $15^{\circ}$  N,  $86^{\circ}$  E, fully established in February (see Figure 5a). This gyre is driven by the northeasterly wind of the winter monsoon. The gyre direction is consistent with the ship drift data of *Cutler and Swallow* [1984] and the observations of *Wyrski* [1961] and *Tchernia* [1980]. The gyre intensifies on the western side, along the coast of India as it travels northward. The appearance of this western boundary current is evident in satellite SST images of the area [*Legeckis*, 1987]. The buoy data of *Molinari et al.* [1990] reveals the gyre but does not show the western recirculation area. This may simply be due to the fact that the small width of the western boundary current could not capture a drifter long enough to trace it. The flow is somewhat barotropic, as evident by the similarity with the second layer results (Figure 6a). The center of the gyre appears at second layer results (Figure 6a). The center of the gyre appears at

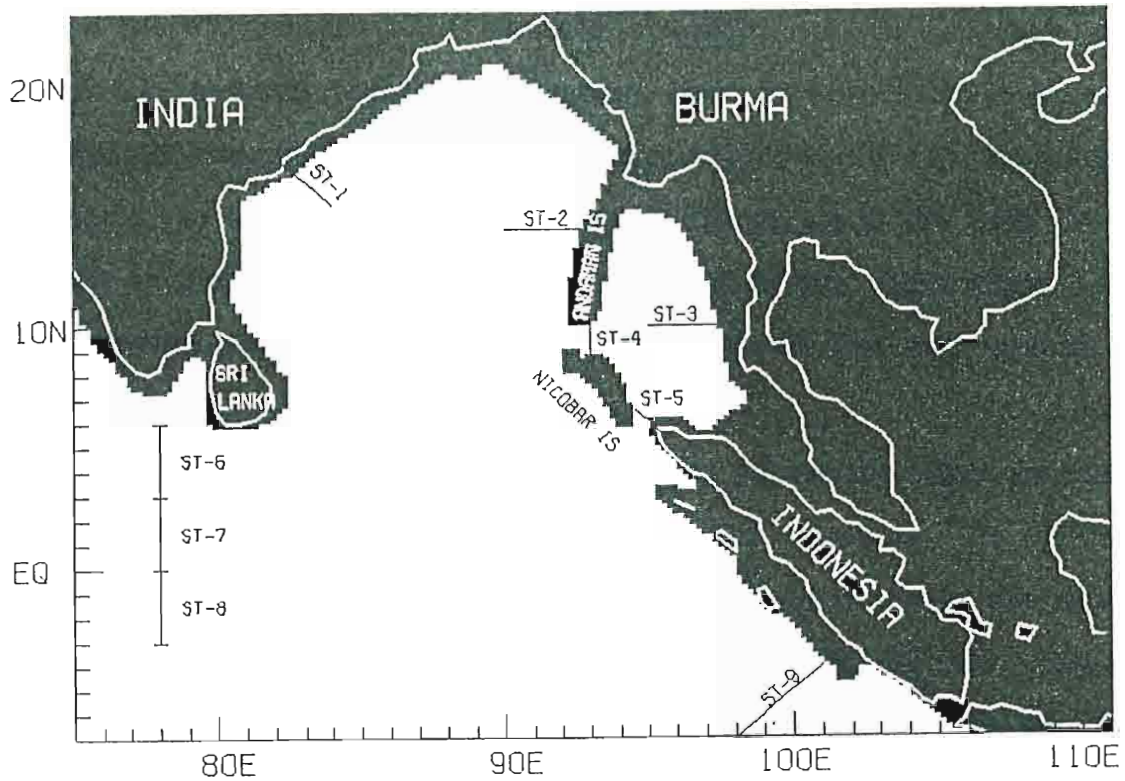


Figure 7. Transect locations. Mass transport through nine stations is computed using model derived data. The first two stations (ST-1 and ST-2) are chosen to investigate flow in the Bay of Bengal. Three other stations (ST-3, ST-4, and ST-5) give an indication of flow in the Andaman Sea. The final four transects (ST-6, ST-7, ST-8 and ST-9) measure the equatorial flow. Three other stations (ST-3, ST-4, and ST-5) give an indication of flow in the Andaman Sea. The final four transects (ST-6, ST-7, ST-8, and ST-9) measure the equatorial flow.

the thickest part of the two model layers. The thickness is 460 m at the center of the circulation ( $14^{\circ}$  N,  $82^{\circ}$  E).

In March (Figure 5b), the anticyclonic gyre is still evident in the model results. The western boundary current is much more narrow, however. Along the coast flow is northward, but a few hundred kilometers off shore, and across the whole bay, it is to the south. In addition, the upper layer thickness along the coast is less than in February, corresponding to a rise in the thermocline. This upwelling region extends along the coast all the way around the bay.

Flow in the lower layer (Figure 6b) shows the same narrowing of the gyre but also the formation of another. A cyclonic circulation has developed in the lower layer directly to the east of the first. It is centered at approximately  $13^{\circ}$  N,  $87^{\circ}$  E. The two gyres are joined at their southward branch, about 300 km from the coast of India.

Two months later, in May (Figure 5c), this upper layer appears unchanged, with upwelling along the coast somewhat less than earlier in the year. In the second layer the flow has reversed direction to a cyclonic orientation. The eastern gyre of the previous month has expanded westward and overridden the anticyclonic gyre that was there. This motion is being fed strongly by the eastward flow around the southern tip of Sri Lanka. The  
by the eastward flow around the southern tip of Sri Lanka. The

flow in May is more baroclinic, therefore, with flow in the upper layer opposing flow at deeper depths.

The flow in the next month, June, as displayed in Figures 5d and 6d, is even more baroclinic. The upper layer flow is northward along both coastlines. At about  $17^{\circ}$  N these two flows meet and turn south. A cyclonic circulation is thus established in the eastern portion of the bay with anticyclonic flow directly to the west. This resembles the subsurface flow of the previous month. The upwelling region along the coast has propagated to the southern end of India, and it is followed by an area of downwelling; a region of deep upper layer thickness (200 m) is evident off the coast of Burma.

The cyclonic circulation flows around an area of shallow thickness; the interface depth is at a minimum of 440 m at the center of the gyre. By August, this area has moved north and hit the coast (Figure 6e). The anticyclonic flow in the lower layer extends over most of the bay. The circulation in the upper layer during August (Figure 5e) is not quite the same as in the second layer. Flow is cyclonic throughout the entire bay. The region of downwelling has progressed westward around the top of the bay. Also, a region of upwelling has propagated northward around Sri Lanka. The upper layer thickness reaches a minimum of 175 m east of the island.

-----  
east of the island.



Toward the end of the year (Figures 5f and 6f), there is weak flow in both layers. The upper layer contains two rotating flows. One, anticyclonic around a region of downwelling, is in the northeastern corner of the bay. Flow along this large eddy is no more than a few centimeters per second, but this will develop into the large, bay-wide circulation of late winter (Figure 5a). In the southwest corner, a cyclonic circulation has developed around a region of upwelling centered at  $10^{\circ}$  N,  $82^{\circ}$  E.

Four stages of the flow in the Bay of Bengal emerge. The first is a large, anticyclonic gyre across the whole bay. This appears throughout the winter months (December until March). This is followed by two, counter-rotating flows, anticyclonic on the western side and cyclonic on the eastern side, producing northward currents along both coasts and southward flow down the middle. This persists until early summer (April through June) when the anticyclonic region dissipates and the cyclonic flow extends across the whole bay. The summer months of July and August are characterized by this large counterclockwise flow. In the fall, two rotating flows develop again, with southward currents along both coasts and northward flow in the center.

This pattern can be seen more quantitatively with the time series plots of mass transports of Figure 8. Transport is measured, using model data, at two transects on opposite sides of the bay (ST-1 and ST-2 of Figure 7). In this case, positive transport is northward along the western coast and southward along the eastern coast. This pattern is also seen in the time series plots of mass transports using model data, at two transects on opposite sides of the bay (ST-1 and ST-2 of Figure 7). In this case, positive transport

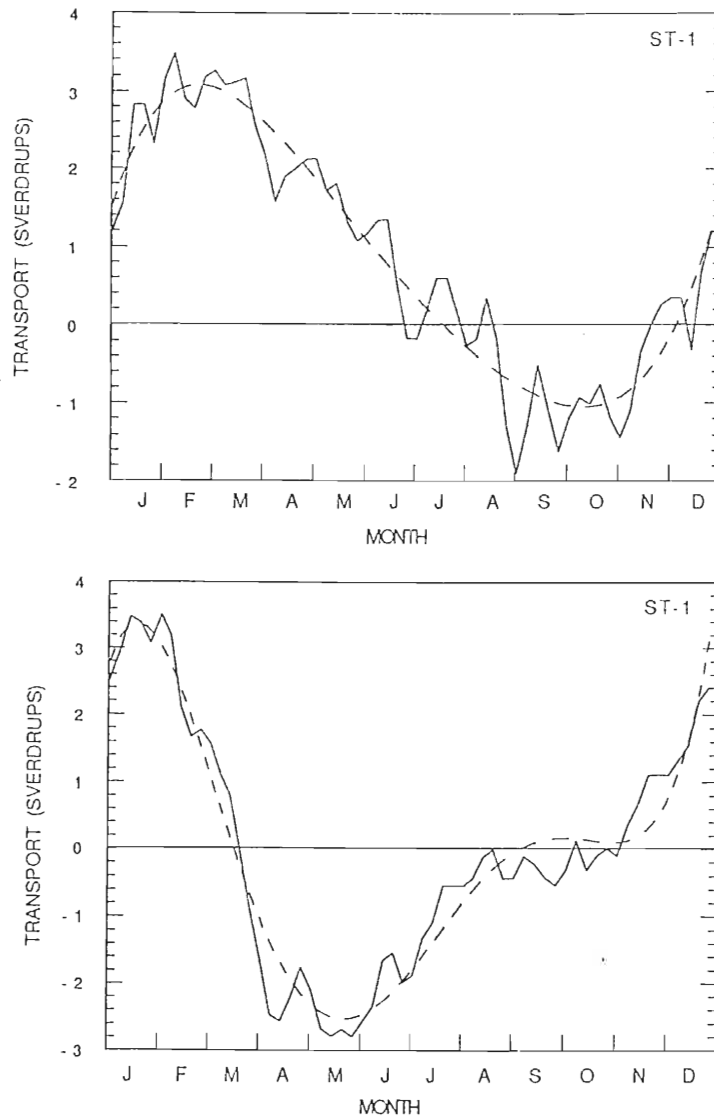


Figure 8. Mass transport in the Bay of Bengal. Transport is calculated, in Sverdrups, using the model velocity and height data. Flow through ST-1 and ST-2 (see Figure 7) are displayed as functions of days. Positive transport indicates northward flow, while negative transport shows southward flow. Transport for the surface layer is above with the second layer below. The raw data were fit with a fifth order polynomial (shown as dashed line). Maximum transports in the upper layer, about 3.5 Sv, are seen in the western boundary current during February.

were fit with a fifth order polynomial (shown as dashed line). Maximum transports in the upper layer, about 3.5 Sv, are seen in the western boundary current during February.

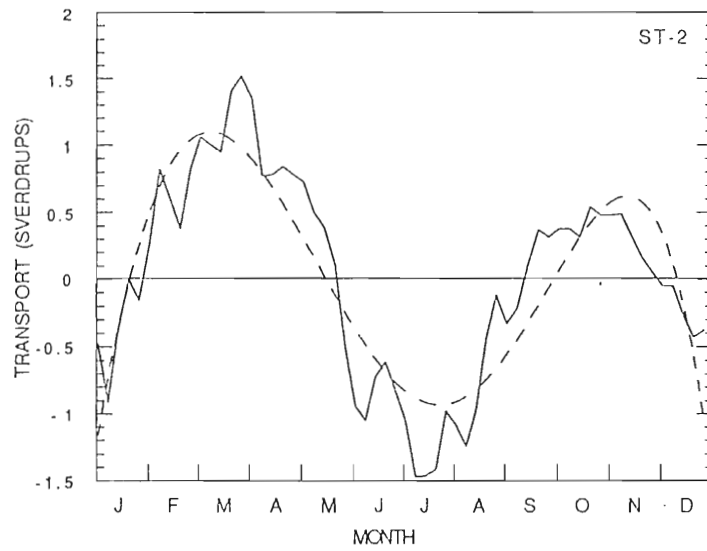
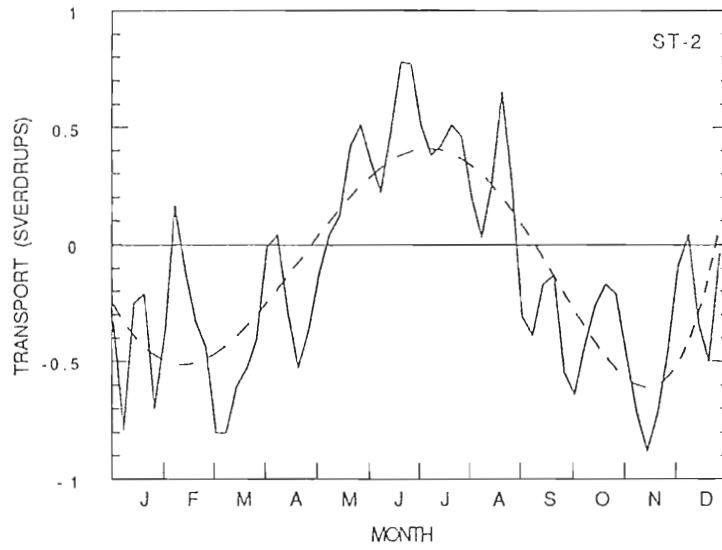


Figure 8. Continued.

Figure 8. Continued.

indicates northward flow, and negative transport reflects southward flow.

The four stages of the circulation are evident from these time series. The bay-wide, anticyclonic circulation of winter is apparent from the positive transport through ST-1 (northward flow) and the negative transport at ST-2 (southward flow). This occurs from December to March. Maximum transport along the western boundary current is 3.5 Sv during February in the upper layer. In the spring months of April, May and June two gyres are present, characterized by positive transport through both ST-1 and ST-2. Maximum transport at this time is 2 Sv in the western boundary. The other flow is very weak, with transport less than 1 Sv along the eastern coast. The eastern, cyclonic gyre expands westward, drowning out the anticyclonic flow and encompasses the whole bay. In July and August transport is northward on the eastern side and negative on the western side. Maximum transport again is along the western boundary, and it reaches -1.29 Sv in late August. Finally, in the fall (September through November) the two gyre system returns, this time with an anticyclonic circulation on the east side and cyclonic in the west. Transport reaches -2.0 Sv during early September in the western boundary current.

The transport calculated in the second layer reveals the baroclinicity of the circulation. The second layer anticyclonic gyre persists in December and January. Maximum transport occurs in baroclinicity of the circulation. The second layer anticyclonic gyre persists in December and January. Maximum transport occurs in

the western boundary, reaching a value of 3.5 Sv in January. In February and March, while the upper layer still has southward flow along the eastern side of the bay, the lower layer begins to show northward (positive) transport on both sides. This develops into cyclonic flow in April and May. In June, July and August flow is southward along both coasts, similar to the two gyre system of the upper layer in fall. Finally in September, October and November the flow is cyclonic throughout the whole bay.

#### 4.2 *The Andaman Sea*

The flow in the Andaman Sea is less complicated than the flow in the Bay of Bengal. In March (Figure 5b) flow in the upper layer enters the sea below the Nicobar Islands, circulates counterclockwise around the Andaman Basin and exits below the Andaman Islands. This pattern continues until July. Figures 5e, 5f, and 5a show that from July until the spring (March) flow enters the basin from the north, circulates clockwise, and exits in the south.

The results in the lower layer are somewhat different. Flow changes direction three times during the year instead of once. In January, February, and March (Figures 6a and 6b) flow is cyclonic. This switches in spring and early summer (April to July). August, September and October show flow returning to a cyclonic  
September and October show flow returning to a cyclonic

orientation. Finally, in November and December (Figure 6f) flow is anticyclonic.

More interesting is the height field in this area. In February a region of upwelling enters the Andaman Sea from the south. The upper layer thickness is 180 m along the southeast coast of the basin. The anticyclonic circulation surrounds a high value of upper layer thickness, 195 m. By March the downwelling region has propagated along the basin coastline and extends well into the Bay of Bengal. The downwelling pulse is followed in May by an area of upwelling. The center of the circulation, now cyclonic, is 180 m deep in the upper layer, and the upwelling signal along the coast reaches 195 m.

By June the upper layer is 215 m deep on the eastern side of the sea, stretching northward along the coast. Finally, in August, the center of the Andaman Sea is marked by a relatively deep mixed layer, 210 m, and flow is anticyclonic around it.

In the lower layer, flow in February is anticyclonic around a relatively thin region, 436 m. The southeast corner of the basin shows a thickening of the top two layers to about 450 m. This thick region, by May, has propagated around the whole sea, increasing to 460 m. In May, the maximum thickness is in the center of the basin, and flow is anticyclonic around it. A region of upwelling then follows in June, propagates up the coast, and moves to the center of the basin by fall.

The calculations of mass transport in this area, made at locations ST-3, ST-4, and ST-5 (see Figure 7) are shown in Figure 9. Maximum transport along the east side of the sea, in the upper layer, is 2 Sv northward in mid May and 1.5 Sv southward in early August. Transports in the lower layer reach 2 Sv in May, but the flow is southward, and in February the flow is northward.

Flow through the Great Channel (southern entry of the Andaman Sea) peaks in May as well, reaching 3.5 Sv northward in the upper layer. Flow exiting the sea in the upper layer becomes 5 Sv in early August. The lower layer experiences northward transport through ST-5 in late February and early March (about 4.2 Sv). The maximum southward flow in this layer, 4 Sv, is during May and June.

#### 4.3 *Equatorial Currents*

The final components of flow in this region are the currents in the equatorial region from  $8^{\circ}$  N down to  $7^{\circ}$  S. During the year three distinct flows are generated in this area. In February, the upper layer shows (Figure 5a) currents flowing toward the west between Sri Lanka ( $6^{\circ}$  N) and  $1^{\circ}$  S. Below  $1^{\circ}$  S the flow is towards the east. The region centered at the equator, from  $3^{\circ}$  N to  $3^{\circ}$  S, is more thin (180 m) than the region just above and below (185 m). A region of downwelling (upper layer thickness about 195 m) can be seen emerging from below Sumatra at  $101^{\circ}$  E. A region of downwelling (upper layer thickness about 195 m) can be seen emerging from below Sumatra at  $101^{\circ}$  E.

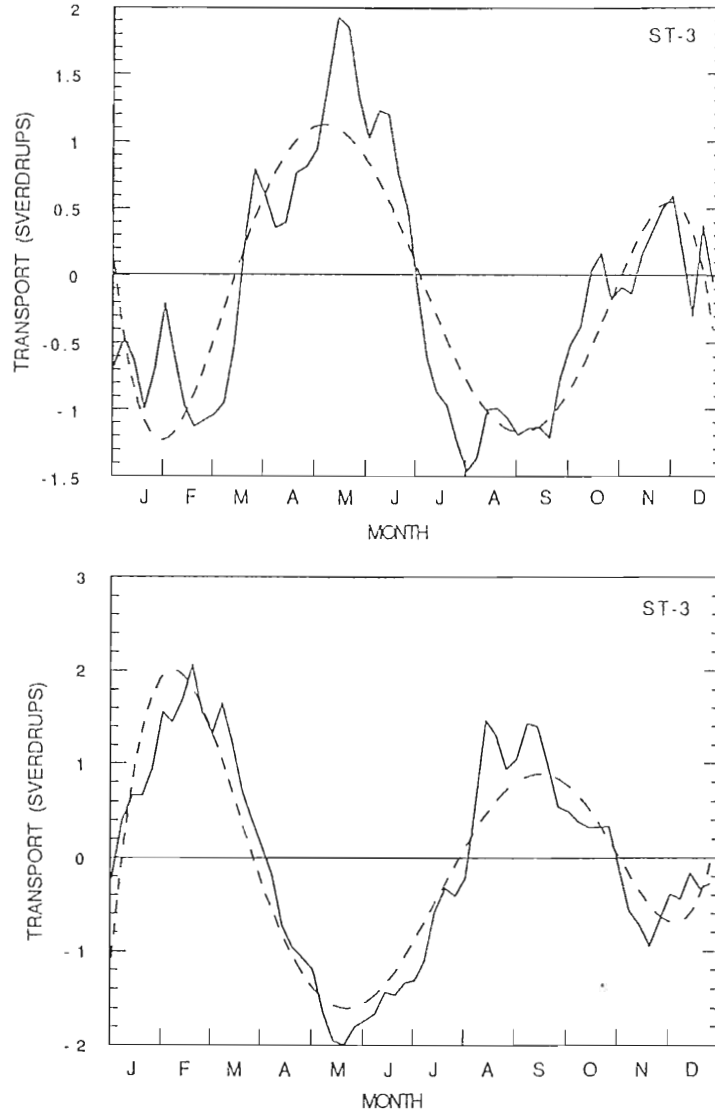


Figure 9. Mass transport in the Andaman Sea. Transport is calculated, in Sverdrups, using the model velocity and height data. Flow through ST-3, ST-4 and ST-5 (see Figure 7) are displayed as functions of days. Positive transport indicates northward flow through ST-3 and ST-5 and eastward flow into the basin through ST-4. Results for the upper layer are above and the lower layer below. The data was fit with fifth order polynomials (dashed line). A semiannual signal is seen in both layers. The two layers are not in phase, however. Maximum transport is seen in the upper layer during May and August, and in the lower layer during February and May.

in phase, however. Maximum transport is seen in the upper layer during May and August, and in the lower layer during February and May.



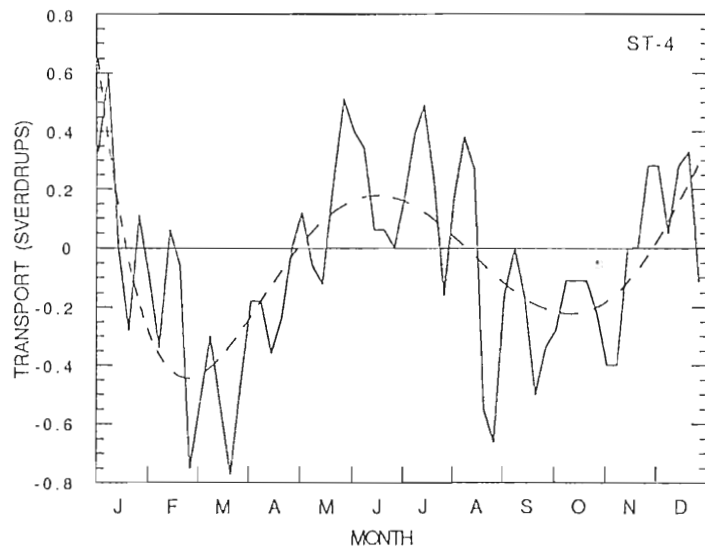
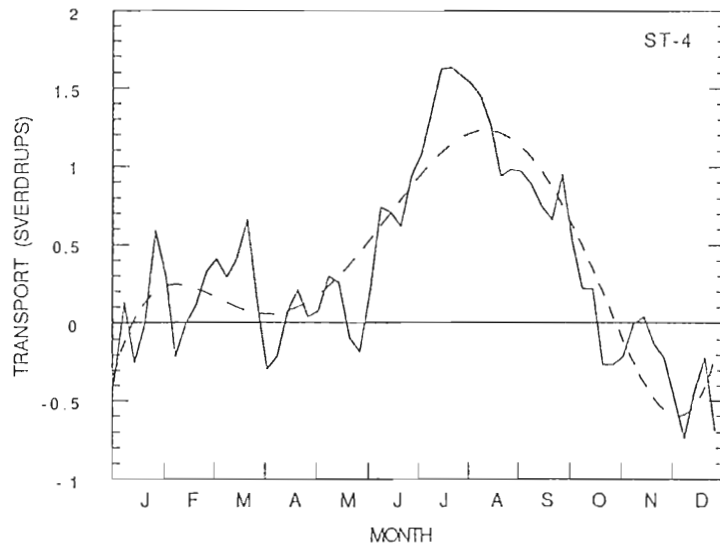


Figure 9. Continued.

Figure 9. Continued.

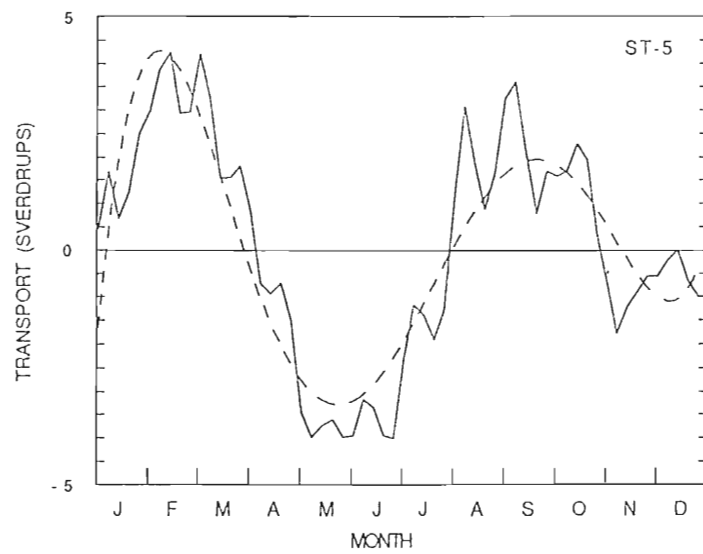
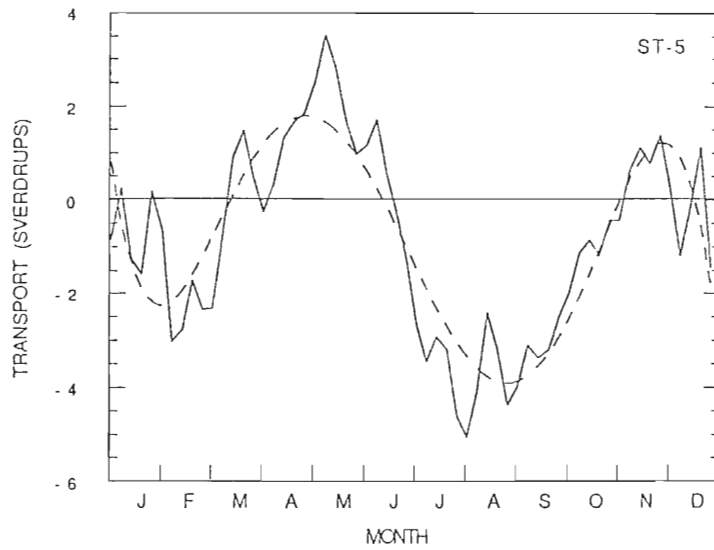


Figure 9 Continued

Figure 9. Continued.

In the next month, March, the thin region at the equator moves off the coast, towards the west, with counterclockwise flow around it. This results in westward flow above  $3^{\circ}$  N and eastward flow from  $3^{\circ}$  N to the equator. Below the equator the flow is still to the east. The downwelling signal, which was off Sumatra in February, leaves the coast at the equator propagating westward. By May (Figure 5c), this signal has moved all the way across the region to  $75^{\circ}$  E. The upper layer thickness on the eastern side has increased to 200 m. The counterclockwise gyre north of the equator has moved to  $78^{\circ}$  E. Flow above  $4^{\circ}$  N is weakly to the east while all other equatorial currents are to the west. In June, the flow starts to follow the upper layer thickness contour, moving toward the east but splitting at about  $80^{\circ}$  E. Flow above the equator is toward the east, while below the equator it is more in a southeast direction. Along the equator the flow is impeded by the thickening of the layer and turns south. The upper layer thickness reaches a maximum along the coast (210 m) this month, however the region is beginning to decrease. By August, as shown in Figure 5e an area of upwelling occurs at  $78^{\circ}$  E. The downwelling pulse moves towards the coast at this time as well. Flow below  $4^{\circ}$  S is to the west. Above  $4^{\circ}$  S, up to  $3^{\circ}$  N, the flow is to the east. Above  $3^{\circ}$  N flow is again in the westward direction. Finally, in November, the equatorial flow to the east strengthens while the westward flow in the north weakens. In December, the equatorial flow to the east strengthens while the westward flow in the north weakens.

The second layer results show a relatively strong equatorial jet established in February. Flow within  $2^\circ$  of the equator is rapid, toward the east. Flow above and below this region is weakly to the west. The region of high velocity is marked by a deep interface depth. In March the flow appears to reverse at about  $85^\circ$  E. More to the east, two regions of deep layer thickness (457 m) develop, symmetric about the equator, with clockwise flow around the one above the equator and counterclockwise flow around the southern one.

In May the two circulations have expanded across the region, producing strong westward flow at the equator and eastward flow above and below. This continues in June, with an upwelling signal, coming from the south, propagating to the north. At the equator, the signal splits, with a large pulse traveling westward to the west and a smaller portion continuing north. Later in the summer, in August, two circulations develop around areas of low depth (440 m), counterclockwise in the north and clockwise in the south. There is strong eastward flow at the equator where the two systems meet. At the end of the year, in November, the flow is relatively weak, and at the equator it is toward the west.

The calculations of transport in the equatorial region, shown in Figure 10, show semiannual periods at all stations except in the upper layer above  $3^\circ$  N which is annual. It also becomes apparent that flow is out of phase in the two layers, as seen in the other upper layer above  $3^\circ$  N which is annual. It also becomes apparent that flow is out of phase in the two layers, as seen in the other

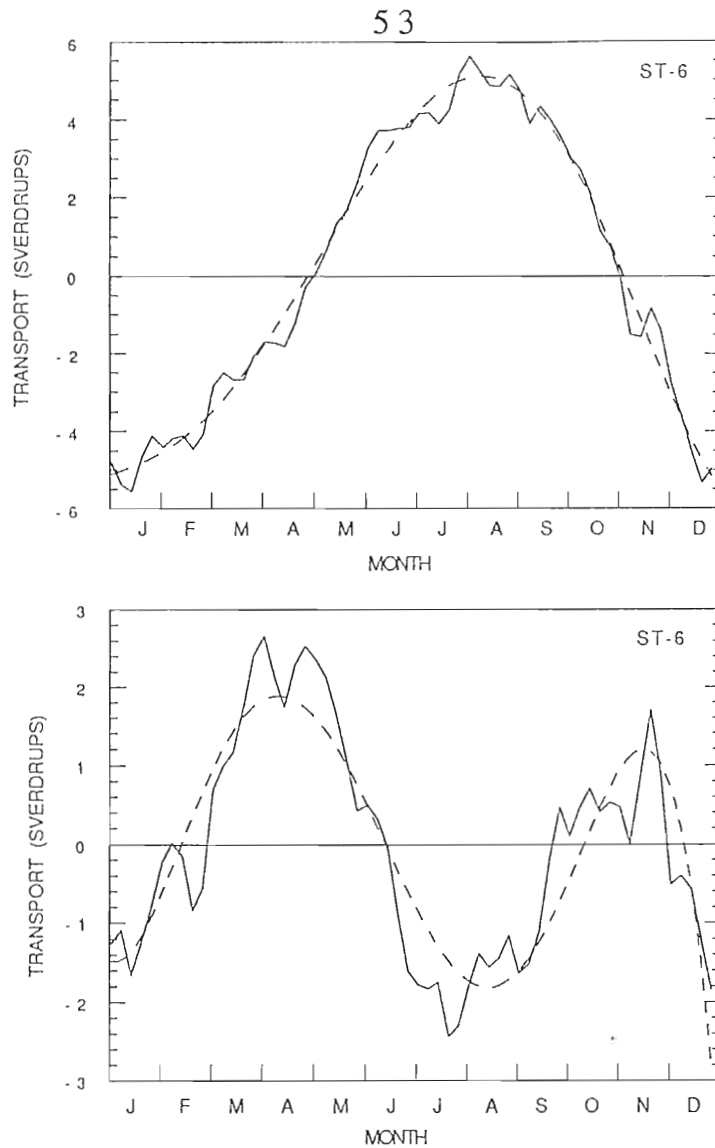


Figure 10. Mass transport in the equatorial region. Transport is calculated, in Sverdrups, using the model velocity and height data. Flow through ST-6, ST-7, ST-8 and ST-9 (see Figure 7) are displayed as functions of days. Positive transport indicates eastward flow through ST-6, ST-7 and ST-8 and northward flow into the basin through ST-9. The data were fit with fifth order polynomials (dashed line). A semiannual signal is seen in both the upper layer (above) and the lower layer (below). Similar to other areas, the two layers are not in phase. Maximum transport at the equator is seen in the upper layer during May, and in the lower layer during February and May.

equator is seen in the upper layer during May, and in the lower layer during February and May.

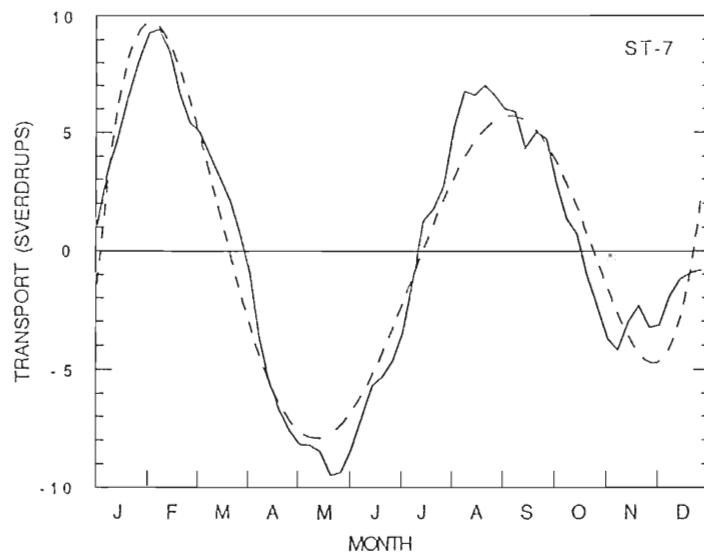
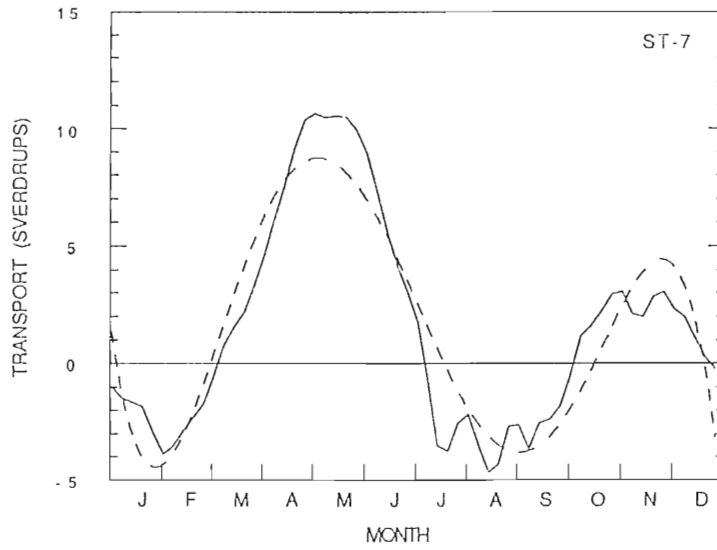


Figure 10. Continued.

Figure 10. Continued.

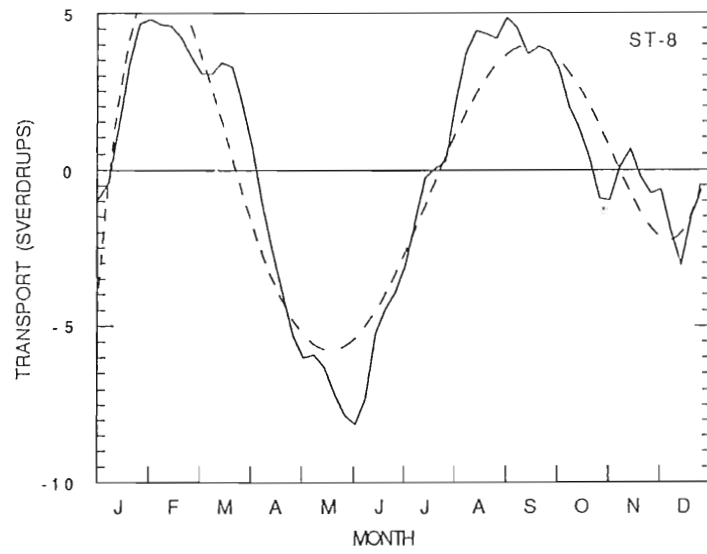
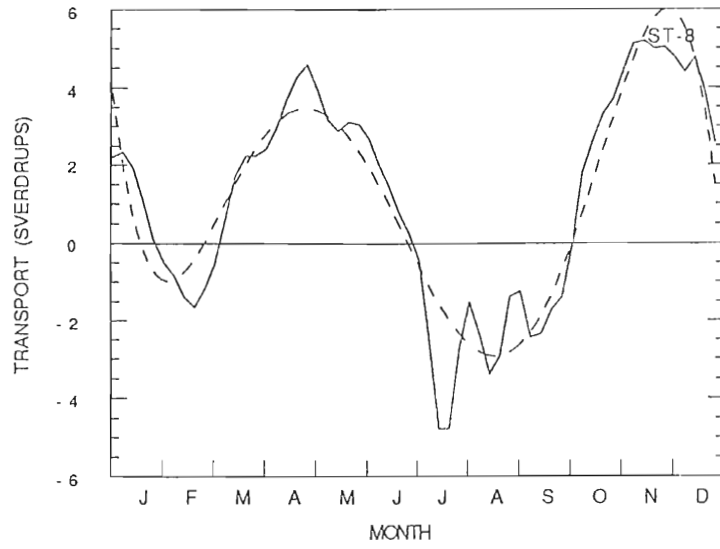


Figure 10. Continued.

Figure 10. Continued.

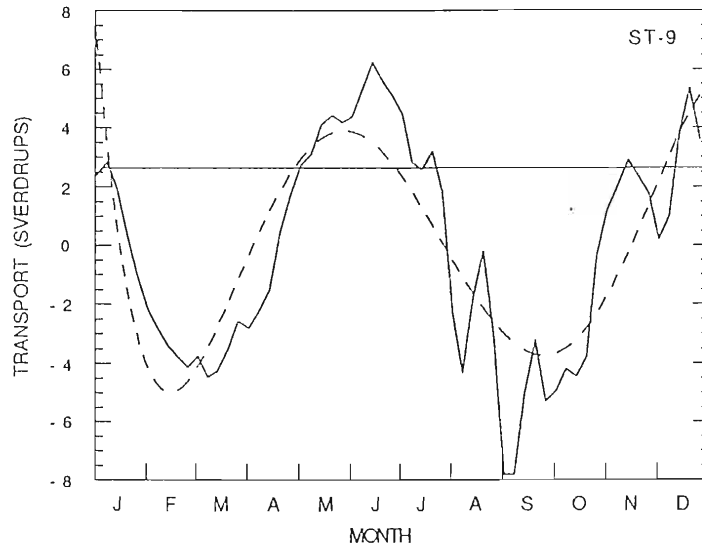
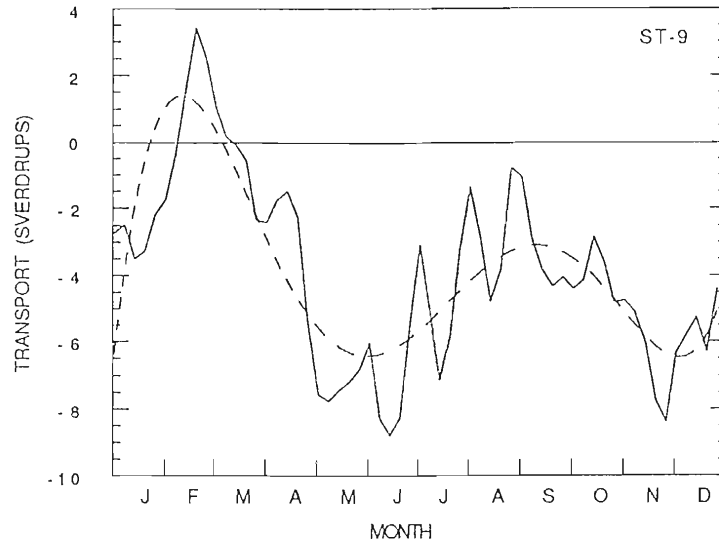


Figure 10. Continued.

Figure 10. Continued.



regions. From  $3^{\circ}$  N to  $6^{\circ}$  N, ST-6, the flow is baroclinic during most of the year. In the upper layer the transport is toward the east from May through October. It reaches a maximum of 5.5 Sv in August. During the rest of the year, November through April, it is to the west, with a maximum of 5.5 Sv in January. The lower layer, however, has net transport eastward during March, April, and May and again in October and November. The maximum during this time is 2.5 Sv during April. During the remainder of the year transport is to the west. The maximum is 2.5 Sv during July.

Lower south, between  $3^{\circ}$  N and the equator (ST-7), shows greater transport. In the upper layer, from March through June and October through December, the transport is to the east. Throughout the month of May it exceeds 10 Sv. The maximum westward flow, 4.5 Sv appears in August. At the same location in the second layer, eastward flow is found during January, February and March and again in August, September and October. The largest eastward transport is in February, 9.5 Sv, and the largest westward transport, again 9.5 Sv, is in May.

Finally, below the equator to  $3^{\circ}$  S (ST-8), transport in the upper layer is shown to be westward during July, August and September, and again in February, in the upper layer. In the lower layer, flow is to the west in April, May, June and July, and again in November, December and January. Maximum transport in

the upper layer is 5 Sv to the east in November, and 5 Sv to the west in late July. The second layer is somewhat more with 8 Sv westward in early June and 5 Sv in late August and again in early February.

## 5. TEMPORAL VARIATIONS

Using various techniques, the time varying signals of the model can be explored. Many elements of the Indian Monsoon system are periodic, ranging from the diurnal signal in rainfall to the annual shift in the winds [*Krishnamurti*, 1976]. These oscillations in the atmospheric conditions create oscillations in the oceanic system. It is also true that oscillations in the ocean can bring about fluctuations in the atmosphere, although atmospheric conditions are not incorporated in the model.

The most obvious signal associated with the monsoon region is the annual reversal in currents associated with the changing monsoon winds. As previously discussed, currents in the Bay of Bengal, the Andaman Sea and in the equatorial region change direction at least once, sometimes twice, during the year. Spectral analysis of the transport data shows that in addition to these annual and semiannual signals there are other major frequencies inherent to the major current systems as reproduced by the model. Two significant peaks in the spectra of the transport time series appear in the 20 to 30 day range and in the 50 to 60 day range. The northern currents in the upper layer, including the eastern and western coasts of the Bay of Bengal, flow in the Andaman Sea, and western coasts of the Bay of Bengal, flow in the Andaman Sea,

and the North Equatorial Current, all show peaks around 23 days. This same peak is seen at all stations (Figure 7) in the lower layer.

The equatorial currents show a peak at a 30 day period in the upper layer and a 26 day peak in the lower layer. Another strong signal is evident at a 60 day period in the equatorial region of both layers. This peak is found in the northern points at a somewhat shorter period, 50 days.

It has been suggested that oscillations of this order, which are found in the tropical Indian ocean, are forced by atmospheric oscillations of similar frequency [*Madden and Julian, 1972*]. The model, however, reproduces these oscillations despite being forced by monthly mean winds. The fundamental period resolved in the wind forcing, therefore, is 60 days.

Effects on a seasonal scale also appear with the formation of waves at the equator and along the coast. An upwelling Kelvin wave, characterized by low upper layer thickness, appears in the model during early winter (Figure 5a). Traveling east along the equator, it hits the coast and reflects back as a downwelling, westward propagating Rossby wave. The maximum amplitude of this wave is seen leaving the coast of Sumatra in early summer (Figure 5d). Some of the energy of the Kelvin wave moves along the coast as two coastal Kelvin waves, one northward and the other southward. This signal can be found propagating the entire coast southward. This signal can be found propagating the entire coastline around both the Andaman Sea and the Bay of Bengal.

A time-longitude plot shows that, as these Kelvin waves travel along the coast, they excite Rossby waves which travel across the basin. In Figure 11a, zonal velocity is plotted since the configuration of the coast at  $18^\circ$  N is mainly in the east-west direction. One significant feature of this picture is the northwest/southeast sloping contour lines in the center of the region,  $87^\circ$  E to  $93^\circ$  E. The tilt indicates a westward propagating feature. Calculation of the slope of this line, in  $\text{m s}^{-1}$ , yields the phase velocity of the westward signal at  $0.035 \text{ m s}^{-1}$ . Gill [1982] calculates that Rossby waves at  $18^\circ$  N will propagate west with a phase velocity of  $0.047 \text{ m s}^{-1}$ . This suggests that the signal appearing in the center of this plot is a Rossby wave that has been generated on the east coast of the bay.

The signal is lost on the western side of the bay as it interacts with the western boundary current. This western intensification appears in the contour plot between  $85^\circ$  E and  $86^\circ$  E. In the first half of the year, January to June, the flow is in the eastward direction. In February and March it reaches a maximum of  $0.120 \text{ m s}^{-1}$ . In June the flow switches direction and remains westward until December. The current is slightly weaker at this time of the year, with maximum velocity  $0.080 \text{ m s}^{-1}$  (westward).

A plot of the upper layer height field, Figure 11b, shows similar features. The westward sloping lines are again evidence of the Rossby wave generated in the east coast. The peaks in the similar features. The westward sloping lines are again evidence of the Rossby wave generated in the east coast. The peaks in the

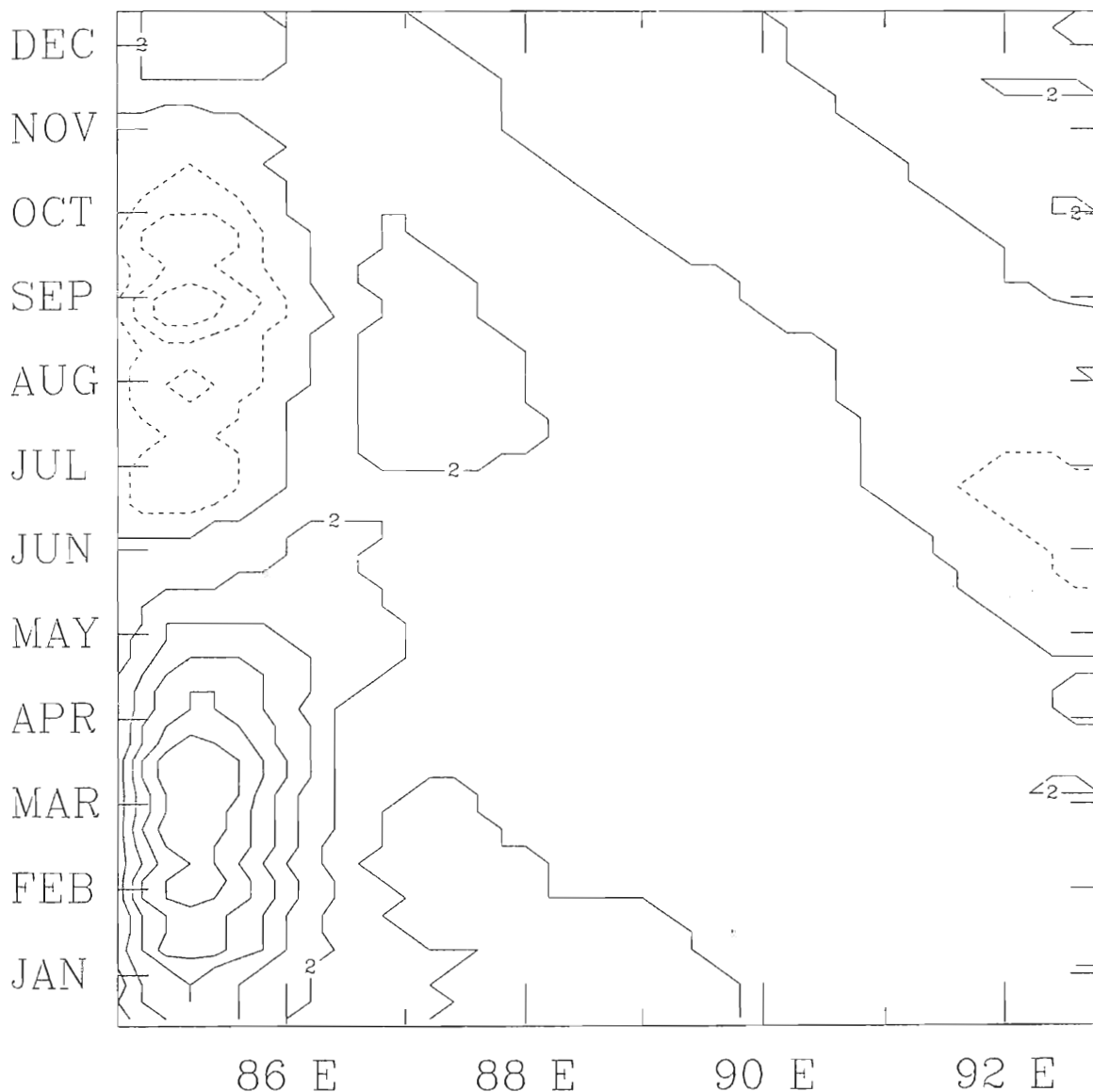


Figure 11a. Zonal velocity in the upper layer at  $18^\circ$  N. The contour values are from  $-0.080 \text{ m s}^{-1}$  (westward) to  $0.120 \text{ m s}^{-1}$  (eastward) at an interval of  $0.020 \text{ m s}^{-1}$  (dashed contour lines indicate westward flow). The annual change in direction of the western intensified current can be seen between  $85^\circ$  E and  $86^\circ$  E. The sloping contours indicate a wave traveling with western phase speed, calculated to be  $0.035 \text{ m s}^{-1}$ , with a period of 232 days. This is interpreted as a Rossby wave generated by a Kelvin wave that is traveling along the coast in the Bay of Bengal.

speed, calculated to be  $0.035 \text{ m s}^{-1}$ , with a period of 232 days. This is interpreted as a Rossby wave generated by a Kelvin wave that is traveling along the coast in the Bay of Bengal.

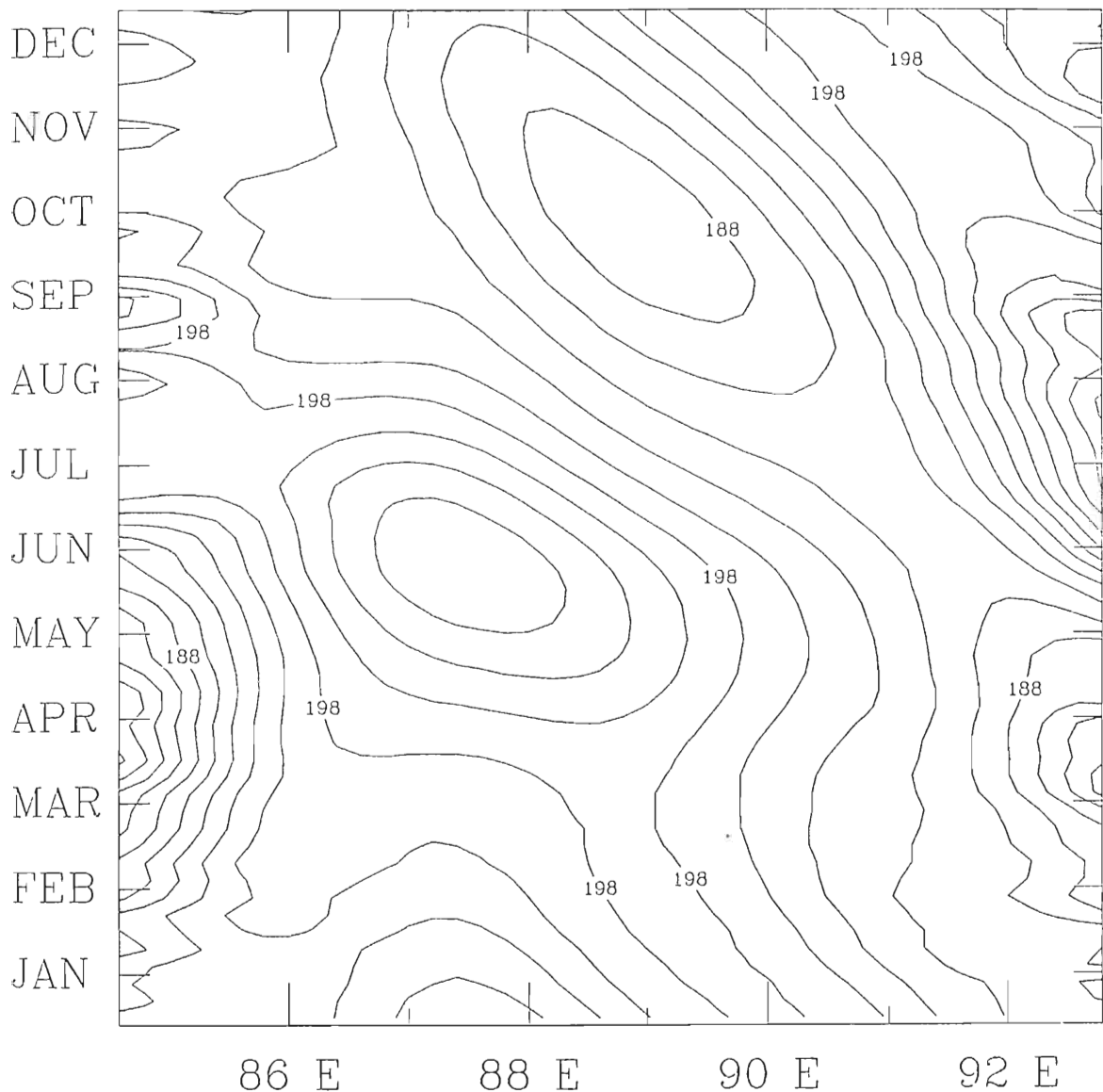


Figure 11b. Upper layer thickness at  $18^{\circ}$  N. The contour values are from 178 m to 208 m at an interval of 2 m. Westward propagating Rossby waves are seen in the summer (upwelling) and again in fall (downwelling). A coastal Kelvin wave is also propagating along the east coast. Westward propagating Rossby waves are seen in the summer (upwelling) and again in fall (downwelling). A coastal Kelvin wave is also propagating along the east coast.

contours in the eastern side of the bay show the coastal Kelvin waves which excite the Rossby waves. These Kelvin waves bring upwelling from January until May followed by downwelling in June through October. The peaks of the excited Rossby waves can be seen in this figure as they propagate westward.

Repeating this procedure for the second layer, at a lower latitude, reveals a similar result (Figure 12). The coastline at this latitude is more north-south, therefore meridional velocity is used (the intrusion of the Andaman Islands accounts for the gap in the contours in Figure 12 at  $93^{\circ}$  E). Maximum velocity, again found in the western boundary current, is  $0.160 \text{ m s}^{-1}$ . During January, February, and March this current flows to the north, in the lower layer, while in April through August it is southward. The westward propagating Rossby waves are evident. The phase is computed, from the slope of the lines, to be  $0.050 \text{ m s}^{-1}$ . The theoretical value, from Gill [1982], is computed to be  $0.054 \text{ m s}^{-1}$ . The phase speed is higher at this latitude than the previous case (phase speed increases with decreasing latitude).

The results in the Andaman Sea (east of  $92^{\circ}$  E) show the current on the eastern side to be southward in February, March and April and again in September, October and November. During the rest of the year it is to the north.

More oscillations are seen in the equatorial wave guide. This is a region a few degrees wide, depending on the trapping scale of

More oscillations are seen in the equatorial wave guide. This is a region a few degrees wide, depending on the trapping scale of



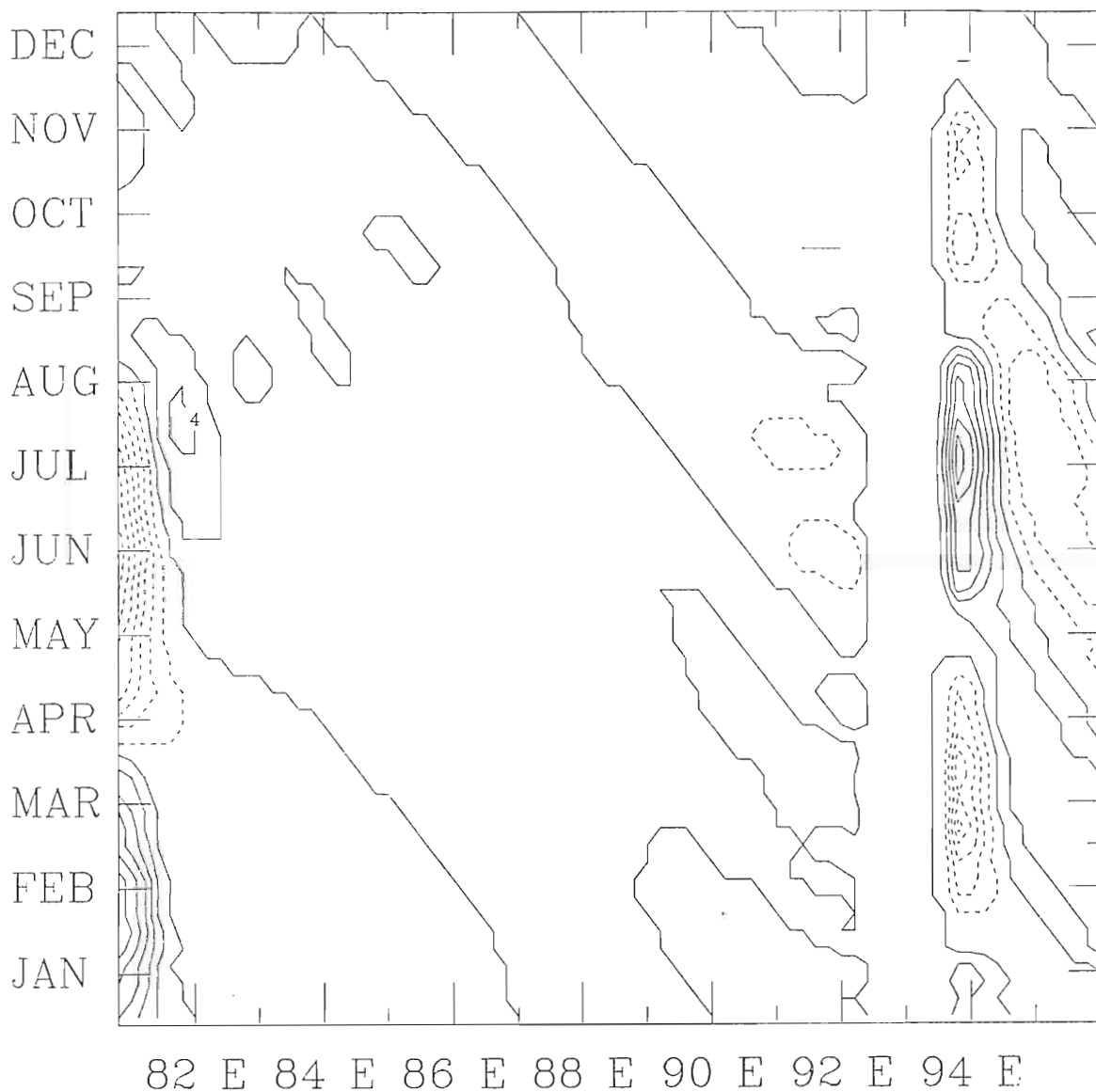


Figure 12. Meridional velocity in the lower layer at  $13^\circ$  N. The contours are from  $-0.160 \text{ m s}^{-1}$  (southward) to  $0.160 \text{ m s}^{-1}$  (northward) at an interval of  $0.020 \text{ m s}^{-1}$  (dashed contours represent southward velocity). The Andaman Islands block the signal between  $92^\circ$  E and  $94^\circ$  E. A westward propagating Rossby wave, generated by a coastal Kelvin wave, appears with phase speed  $0.047 \text{ m s}^{-1}$  and period 200 days as evident in the sloping contours. The western intensification appears to change direction three time during the year (late May, mid August, and late November).

a particular wave, centered at the equator. Waves generated in this region become trapped due to the effects of the Coriolis force. Three of the lower frequency waves (periods greater than two weeks) that propagate in this region are the eastward traveling Kelvin waves, the westward Rossby waves, and westward propagating mixed Rossby-gravity waves (Yanai waves). Figure 13 displays contours, plotted using a color scale, of the antisymmetric component of the upper layer height field along  $3^\circ$  N. The antisymmetric component is computed by subtracting the signal at  $3^\circ$  S from the signal at  $3^\circ$  N. Signals symmetric about the equator are therefore eliminated. The antisymmetric waves include even mode Rossby waves, which have relatively low frequencies, and the higher frequency Yanai waves. The signal in Figure 13 is computed to have a period of 240 days and phase velocity of  $0.190 \text{ m s}^{-1}$ , indicative of a Rossby wave.

At the equator, the higher frequency Yanai waves are seen. Both Figure 14a and 14b (upper and lower model layers, respectively) show a westward propagating feature with phase speed  $0.300 \text{ m s}^{-1}$  and period about 30 days. Using these values in the linear dispersion relationship for equatorial waves, these can be identified as Yanai waves. These waves have been observed in all oceans, and they were first seen in the Indian Ocean by *Luyten and Roemmich* [1982]. *Kindle and Thompson* [1989] in all oceans, and they were first seen in the Indian Ocean by *Luyten and Roemmich* [1982]. *Kindle and Thompson* [1989]

studied Yanai waves in detail using a one and one half layer model of the Indian Ocean.

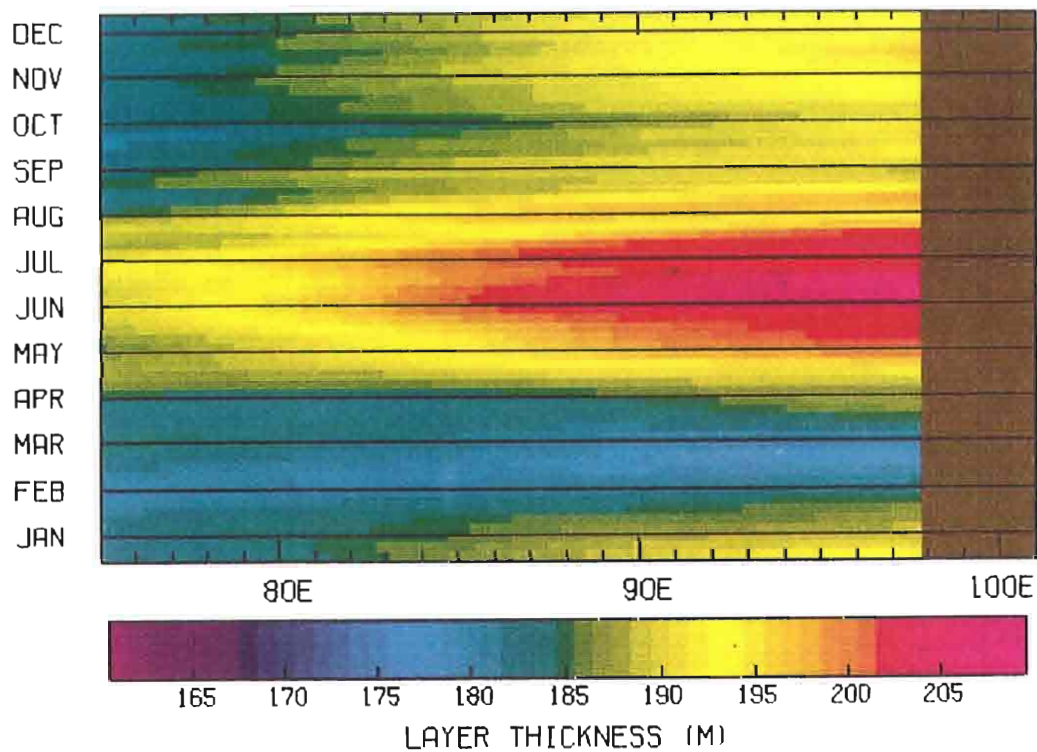


Figure 13. Antisymmetric component of the height field at  $3^{\circ}$  N. The sloping contour indicates a wave traveling west (phase velocity  $0.190 \text{ m s}^{-1}$  to the west and period 240 days). Due to the signal appearing in the antisymmetric plot and the phase velocity, these waves are interpreted as Rossby waves.

velocity  $0.190 \text{ m s}^{-1}$  to the west and period 240 days). Due to the signal appearing in the antisymmetric plot and the phase velocity, these waves are interpreted as Rossby waves.

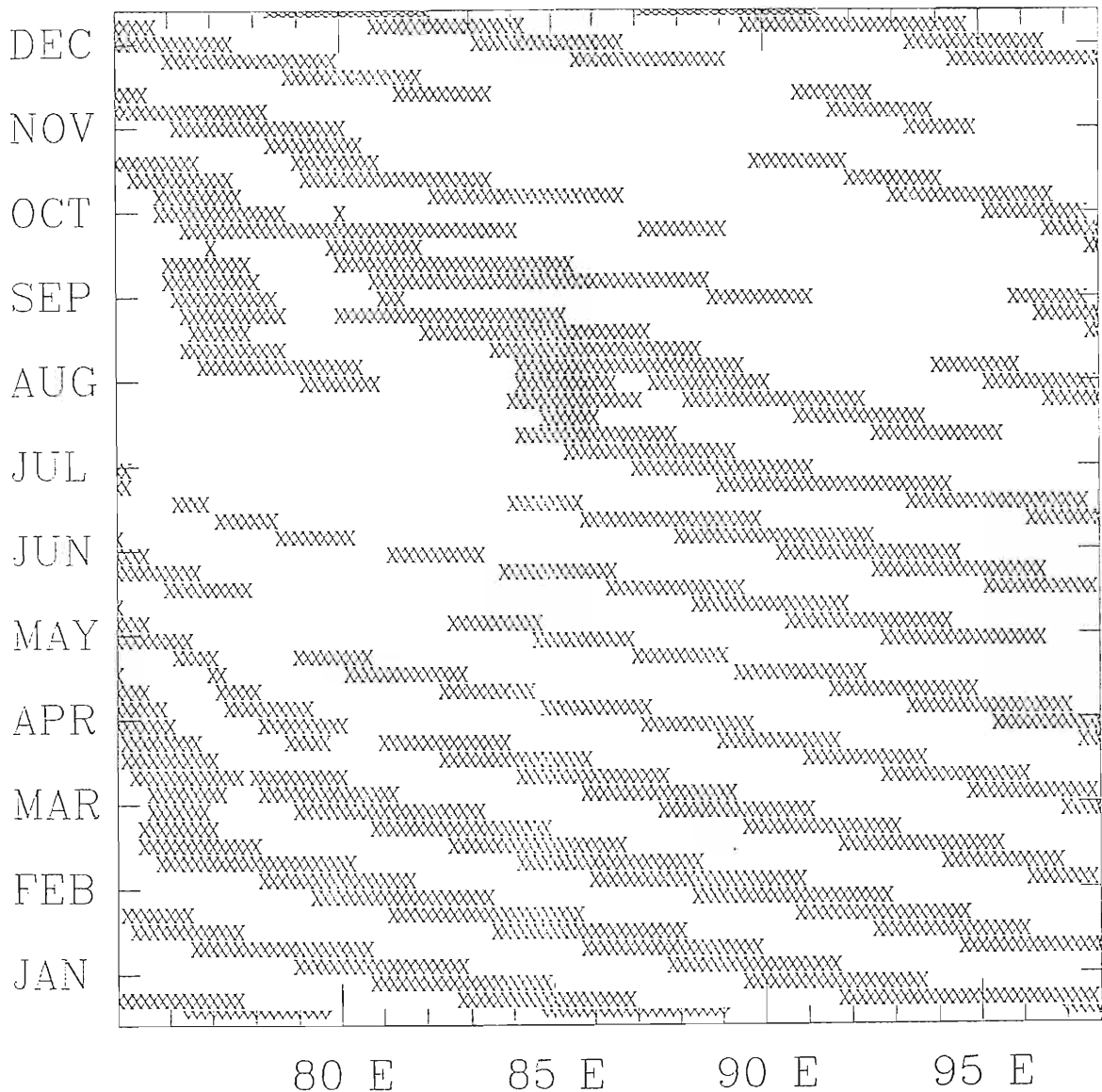


Figure 14. Meridional velocity at the equator for (a) model upper layer, and (b) model lower layer. Velocities are from  $-0.080 \text{ m s}^{-1}$  (southward) to  $0.080 \text{ m s}^{-1}$  (northward). In this representation, areas of southward velocity are shaded. The slope to these areas show features with westward propagation, a phase speed of  $0.300 \text{ m s}^{-1}$  and a period of about 30 days, interpreted as Yanai waves. areas of southward velocity are shaded. The slope to these areas show features with westward propagation, a phase speed of  $0.300 \text{ m s}^{-1}$  and a period of about 30 days, interpreted as Yanai waves.

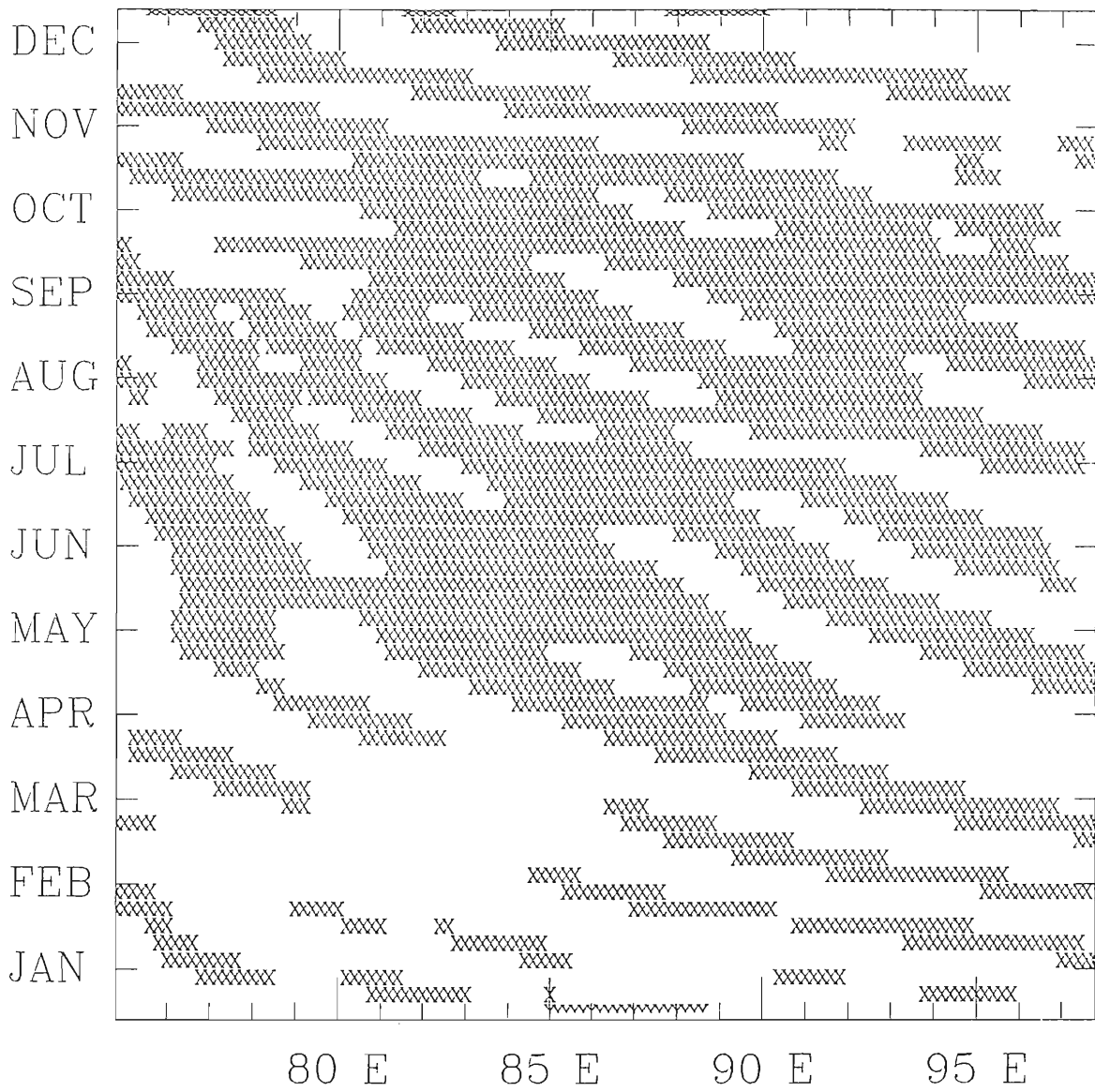


Figure 14. Continued.

Figure 14. Continued.

## 6. CONCLUSIONS

The purpose of this study is to study the seasonal circulation in the Bay of Bengal. Due to the scarcity of measured data in this region, a three and one half layer model, driven by climatological monthly mean winds, is used to examine the dynamics of this region of the Indian Ocean. This model accurately simulates the currents with slight deviations from available observations.

Flow in the Bay of Bengal is observed in the model results to be strongly anticyclonic, in the surface layer, in the winter months of December, January, February and March. In spring and early summer, two circular flows develop, anticyclonic on the western side of the bay and cyclonic on the eastern side. In July and August, the cyclonic circulation extends over the entire basin. Flow at this time is very weak, however. In the fall the two gyre system forms again with the appearance of an anticyclonic circulation in the eastern half of the bay. By winter this flow has moved across the bay and the process repeats itself. The second layer of the model shows a similar pattern, but it occurs slightly out of phase with the surface layer. This circulation pattern is in general agreement with observations. Some assumptions are made since the scale of the model is more detailed than the measured data.

since the scale of the model is more detailed than the measured data.

Oscillations in these currents are illustrated through spectral analysis of transport data in this region. Significant peaks at 20 and 50 day periods are found at both the eastern and western sides of the bay. In addition, the results of the model height field show a coastal Kelvin wave, which originates at the equator, propagating around the entire western perimeter of the region (around both the Andaman Sea and the Bay of Bengal). This wave, when in the bay, excites westward propagating Rossby waves.

Flow in the Andaman Sea is observed to be clockwise in the upper layer during most of the year. In spring and early summer it is counterclockwise. In contrast, flow in the lower layer reverses four times during the year. Measured data in this region is not very abundant, but the atlases that do exist show weak drift currents in the north-south direction fed by the equatorial currents. The model treats this region as more of an enclosed area, so a circular flow can develop. Significant oscillations occur in this region at periods of 25 and 50 days in the surface layer and 20 and 36 days in the lower layer.

Finally, currents in the equatorial region are examined. The NEC, SEC and ECC are all represented by the model. Also, an equatorial jet appears in the monsoon transition periods, consistent with observations. Spectral analysis shows significant peaks at 30 and 60 days periods for currents in this region. Rossby and Yanai with observations. Spectral analysis shows significant peaks at 30 and 60 days periods for currents in this region. Rossby and Yanai



waves are also observed propagating westward in the equatorial wave guide.

## References

- Antony, M. K., C. S. Murty, G. V. Reddy, and K. H. Rao, Sub-surface Temperature Oscillations and Associated Flow in the Western Bay of Bengal, *Estu. Shelf Sci.*, **21**, 823-834, 1985.
- Bahulayan, N. and V. V. R. Varadachari, Numerical Model for Wind Driven Circulation in the Bay of Bengal, *Indian J. Mar. Sci.*, **15**, 8-12, 1986.
- Bigg, Grant R., D. Jiang, and J. F. Mitchell, Preliminary Results from a General Circulation Model of the Past and Present Indian Ocean, *Ocean Modelling*, **86**, 5-8, 1989.
- Cadet, Daniel L., and Bradley C. Diehl, Interannual Variability of Surface Fields over the Indian Ocean during Recent Decades, *Mon. Wea. Rev.*, **112**, 1921-1935, 1984.
- Cane, Mark A., On the Dynamics of Equatorial Currents, with Application to the Indian Ocean, *Deep Sea Res.*, **27A**, 525-544, 1980.
- Cutler, A. N., and J. C. Swallow, Surface Currents of the Indian Ocean (to 25° S, 100° E): Compiled from Historical Data Archived by the Meteorological Office, Bracknell, UK, *Report 187*, 8 pp., 36 charts, Inst. of Oceanogr., Wormley, England, 1984.
- 187, 8 pp., 36 charts, Inst. of Oceanogr., Wormley, England, 1984.

- Düing, Walter, *The Monsoon Regime of the Currents in the Indian Ocean*, 68 pp., East-West Center Press, Honolulu, 1970.
- Fein, Jay S. and P. L. Stephens, eds., *Monsoons*, 632 pp., John Wiley & Sons, New York, 1987.
- Gill, Adrian E., *Atmosphere-Ocean Dynamics*, 662 pp., Academic Press, Orlando, 1982.
- Hastenrath, S., *Climate and Circulation of the Tropics*, 455 pp., Kluwer Academic Publishers, Hingham, 1985.
- Hastenrath, S. and P. J. Lamb, *Climate Atlas of the Indian Ocean, I, Surface Climate and Atmospheric Circulation*, 19 pp., 97 charts, University of Wisconsin Press, Madison, 1979.
- Hellerman, Sol, and Mel Rosenstein, Normal Monthly Wind Stress Over the World Ocean with Error Estimates, *J. Phys. Ocean.*, **13**, 1093-1104, 1983.
- Jensen, Tommy G., A Numerical Study of the Seasonal Variability of the Somali Current, Ph. D. dissertation, 118 pp., Florida State University, February, 1990.
- Johns, B., A. D. Rao, S. K. Dube, and P. C. Sinha, Numerical Modelling of Tide Surge Interaction in the Bay of Bengal, *Phil. Trans. R. Soc.*, **313**, 507-535, 1985.
- Gent, P. R., K. O'Neill, and M. A. Cane, On the Dynamic Formulation of the Large-Scale Momentum Exchange between Atmosphere and Ocean, *J. Mar. Res.*, **24**, 105-112, 1983.
- of the Large-Scale Momentum Exchange between Atmosphere and Ocean, *J. Mar. Res.*, **24**, 105-112, 1983.

- Kindle, John C., and Dana J. Thompson, The 26- and 50-Day Oscillations in the Western Indian Ocean: Model Results, *J. Geophys. Res.*, **94**, 4721-4736, 1989.
- Krishna, V. V. G., and J. S. Sastry, Surface Circulation over the Shelf off the East Coast of India during the SW Monsoon, *Indian J. Mar. Sci.*, **14**, 62-65, 1985.
- Krishnamurti, T. N., and H. N. Bhalme, Oscillations of a Monsoon System. Part I. Observational Aspects, *J. Atmos. Sci.*, **33**, 1937-1954, 1976.
- Legeckis, Richard, Satellite Observations of a Western Boundary Current in the Bay of Bengal, *J. Geophys. Res.*, **92**, 12,974-12,978, 1987.
- Luther, M. E., Indian Ocean Modeling, *Further Progress in Equatorial Oceanography*, edited by E. Katz and J. Witte, pp. 303-316, Nova University Press, Dania, 1987.
- Luther, Mark E., and J. J. O'Brien, A Model of the Seasonal Circulation in the Arabian Sea Forced by Observed Winds, *Prog. Oceanog.*, **14**, 353-385, 1985.
- Luther, M. E., J. J. O'Brien, and A. H. Meng, Morphology of the Somali Current System During the Southwest Monsoon, *Coupled Ocean-Atmosphere Models*, edited by J. C. J. Nihoul, pp. 405-437, Elsevier Science Publishers, Amsterdam, 1985.
- pp. 405-437, ELSEVIER SCIENCE PUBLISHERS, AMSTERDAM, 1985.

- Luyten, James R., and D. H. Roemmich, Equatorial Currents at Semi-Annual Period in the Indian Ocean, *J. Phys. Ocean.*, **12**, 406-413, 1982.
- Madden, R. A., and P. R. Julian, Description of Global-Scale Circulation Cells in the Tropics with a 40-50 Day Period, *J. Atmos. Sci.*, **29**, 1109-1123, 1972.
- McClain, E. Paul, W. G. Pichel, and C. C. Walton, Comparative Performance of AVHRR-Based Multichannel Sea Surface Temperatures, *J. Geophys. Res.*, **90**, 11,587-11,601, 1985.
- Molinari, Robert L., D. Olson, and G. Reverdin, Surface Current Distributions in the Tropical Indian Ocean Derived from Compilations of Surface Buoy Trajectories, *J. Geophys. Res.*, **95**, 7217-7238, 1990.
- O'Brien, James J., The Diffusive Problem, *Advanced Physical Oceanographic Numerical Modelling*, Edited by J. J. O'Brien, pp. 127-144, D. Reidel Publishers, New York, 1986.
- O'Brien, James J., and H. E. Hurlburt, Equatorial Jet in the Indian Ocean: Theory, *Science*, **184**, 1075-1077, 1974.
- Panakala Rao, D. and J. S. Sastry, Circulation and Distribution of Some Hydrographic Properties during the Late Winter in the Bay of Bengal, *Mahasagar*, **14**, 1-15, 1981.
- Piccard, G. L., and W. J. Emery, *Descriptive Physical Oceanography*, 249 pp., Pergamon Press, New York, 1982.
- Piccard, G. L., and W. J. Emery, *Descriptive Physical Oceanography*, 249 pp., Pergamon Press, New York, 1982.

- Rao, Rokkam R., R. L. Molinari, and J. F. Festa, Evolution of the Climatological Near-Surface Thermal Structure of the Tropical Indian Ocean, *J. Geophys. Res.*, **94**, 10,801-10815, 1989.
- Somayajulu, Y. K., T. V. Ramana Murty, S. Prasanna, and J. S. Sastry, Hydrographic Characteristics of Central Bay of Bengal Waters during the Southwest Monsoon of 1983, *Ind. J. of Mar. Sci.*, **16**, 207-217, 1987.
- Subbaramayya, I., and S. R. Rao, Secular Variations of Sea Surface Temperature in the Bay of Bengal, *Mahasagar*, **19**, 165-173, 1986.
- Tchernia, P., *Descriptive Regional Oceanography*, 253 pp., Pergamon Press, Oxford, England, 1980.
- Woodberry, Karen E., M. E. Luther, and J. J. O'Brien, The Wind Driven Seasonal Circulation in the Southern Tropical Indian Ocean, *J. Geophys. Res.*, **94**, 17,985-18,002, 1989.
- Wyrski, K., An Equatorial Jet in the Indian Ocean, *Science*, **181**, 262-264, 1973.
- Wyrski, K., *Oceanographic Atlas of the International Indian Ocean Expedition*, 531 pp., National Science Foundation, Washington, D.C., 1971.
- Wyrski, K., Physical Oceanography of the Southeast Asian Waters, Scientific Results of the Maritime Investigations of the South China Sea and Gulf of Thailand 1959-1961, *NAGA Report 2*, 195  
Scientific Results of the Maritime Investigations of the South China Sea and Gulf of Thailand 1959-1961, *NAGA Report 2*, 195

pp., Scripps Institute of Oceanography, La Jolla, California, 1961.

Yu, Lisan and Jiayan Yang, On the Remote Forcing of the Circulations in the Bay of Bengal, *J. Phys. Ocean.*, in preparation.

### **Biographical Sketch**

James Potemra was born in Palo Alto, California in 1964 and grew up in Washington, DC. He received a B. S. degree in physics from Stevens Institute of Technology in Hoboken, New Jersey in 1986. He was then a member of the research staff of ORI, Inc. in Rockville, Maryland where he conducted studies of submarine control systems for the US Navy at the David Taylor Research Center in Carderock, Maryland. In 1988 he was awarded a NASA Traineeship in Physical Oceanography to pursue graduate work at the Florida State University at Tallahassee, Florida. He obtained a M. S. degree in Physical Oceanography in 1990.